International Journal of Thermofluids 27 (2025) 101256

Contents lists available at ScienceDirect

International Journal of Thermofluids

journal homepage: www.sciencedirect.com/journal/international-journal-of-thermofluids

Experimental and molecular-level insights into thermal conductivity of cobalt hydroxychloride nanofluids

P.T. Ntumba [a], S. Khamlich [b], B.T. Sone [c], V. Fester [d,*]

[a] Department of Chemical Engineering, Cape Peninsula University of Technology, PO Box 1906, Bellville, 7535, South Africa
[b] Applied Chemistry and Engineering Research Centre of Excellence (ACER-CoE), Mohammed VI Polytechnic University, Lot 660, Hay Moulay Rachid, Ben Guerir 43150, Morocco
[c] Chemistry Department, Faculty of Natural & Agricultural Sciences, University of Pretoria, Pretoria, South Africa
[d] Flow Process & Rheology Centre, Faculty of Engineering & the Built Environment, Cape Peninsula University of Technology, Cape Town, South Africa

ARTICLE INFO

Keywords:
$Co_2(OH)_3Cl$ nanoparticles
Brownian motion
Nanofluid
Thermal conductivity
Heat transfer

ABSTRACT

This study reports the influence of shape and size on the thermal conductivity of cobalt hydroxychloride ($Co_2(OH)_3Cl$) nanofluids synthesised via a low temperature hydrothermal precipitation process at varying propanol concentrations ranging from 0 % to 100 %. The structural and morphological properties of resulting powders were analysed using XRD, FTIR, and HRTEM. Thermal conductivity analysis was performed at temperature from 298 K to 318 K using a steady state cylindrical guarded hot plate method. Equilibrium molecular dynamics with the Green–Kubo method were utilised to obtain further insight into the thermal conductivity enhancement, simulating spherical, rhombus nanoplates and a mixed system. XRD confirmed the presence of $Co_2(OH)_3Cl$ with varying purities depending on propanol concentration; higher concentrations (70–100 %) yielded purer phases. Morphological analysis using HRTEM revealed hexagonally shaped $Co_2(OH)_3Cl$ nanoplates with average sizes ranging from 85 to 55 nm at propanol concentrations below 50 %. In contrast, spherical $Co_2(OH)_3Cl$ nanoparticles and rhombus-shaped nanoplates, with average sizes ranging from 23 to 10 nm, were formed at propanol concentrations ranging from 70 % to 100 %. Higher propanol concentration therefore restricts particle growth and promotes shape transition from nanoplates to nanospheres. A reduction in nanoparticle size and rise in temperature resulted in enhancing the thermal conductivity of the obtained nanofluids. At 318 K, a thermal conductivity enhancement of 17.7 % was achieved at nanoparticle sizes below 10 nm. The equilibrium molecular dynamics study confirmed that the observed 17.7 % enhancement in thermal conductivity could be credited to the combination of nanoparticle shapes at very narrow particle sizes. This study highlights the significant impact of nanoparticle size and shape on the thermal conductivity of novel $Co_2(OH)_3Cl$ nanofluids and pave a way to optimising nanofluid performance based on EMD studies prior to synthesis.

Introduction

By definition, heat transfer occurs when energy is transferred from one body to another due to differences in temperatures [1]. Heat transfer is used in devices including solar thermal collectors for converting sunlight into heat [2]. Improved heat transfer increases the heat transfer efficiency of solar collectors [3,4]. Hence, various research works have been conducted to enhance the thermal performance of solar thermal collectors. These reported studies include the use of polymer materials in the construction of collectors and modifications to the geometric design of the absorber plate; the use of selective solar absorbers as coatings for the collectors, etc. [5,6]. An alternative approach to improving solar collector performance is to add nanosised particles (nanoparticles) with higher thermal conductivity to conventional heat transfer fluids to increase their overall thermophysical properties. Nanofluids are suspensions obtained from the dispersion of nanoparticles in a base fluid such as water, various types of glycols, therminol oil, etc. [7]. Because of the potential applications of nanofluids in heat transfer, different types of nanoparticles including metallic (e.g., Pt, Zn, Al, Ti and Mo), metal oxide (e.g., Al_2O_3, Fe_3O_4, CeO_2, CuO, ZnO), single and multi-wall carbon nanotubes (CNT) or graphene and graphene oxide nanosheets were investigated for their influence on the thermal conductivity of nanofluids. Magnetic p-type semiconductors such as cobalt oxide (Co_3O_4) has been used in a wide range of applications, including lithium-ion batteries, gas sensing, electrochromic devices,

* Corresponding author.
E-mail address: FesterV@cput.ac.za (V. Fester).

https://doi.org/10.1016/j.ijft.2025.101256

Available online 17 May 2025

Nomenclatures

ATR-FTIR	Attenuated total reflectance-Fourier transformed infrared spectroscopy
EMD	Equilibrium Molecular Dynamics
EMD-GK	Equilibrium Molecular Dynamics simulation integrated with the Green-Kubo
D	Diameter
ITR	Interfacial thermal resistance
L	Length
MWCNT	Multiwall carbon nanotubes
OD	Outer Diameter
SWCNT	Singlewall carbon nanotubes
TEM	Transmission electron microscopy
UV–VIS-NIR	Ultraviolet, visible, near-infrared spectroscopy
XRD	X-ray powder diffraction
Q	Heat flux rate (W)
HCACF	Heat current autocorrelation function
HFACF	Heat flux autocorrelation function
RDFs	Radial distribution functions
SDS	Sodium dodecyl sulphate
knf	Nanofluid thermal conductivity (W/mK)
kbf	Base fluid thermal conductivity (W/mK)
kB	Boltzmann constant
D	Nanofluid thickness between both cylinders (m)
A	Hot cylinder lateral area (m2)
Th	Inner cylinder temperature (K)
Tc	Outer cylinder temperature (K)
V(rij)	Lennard-Jones (LJ) potential (eV)
rij	Distance between two atoms i & j at minimum energy (Å)
Ei	Sum of potential and kinetic energies (J)

Greek symbols

εij	Potential well depth (eV)
σij	Finite distance where the pairwise becomes 0 (Å)
A	Atom type in the nanofluid system
hα	Enthalpy of atoms present in the nanofluid system
Nα	Number of atoms belonging to the atomic type α

electrochemical systems, and solar selective absorbers [8–12]. One of the methods for producing Co_3O_4 nanoparticles consists in the synthesis of solid cobalt precursors followed by their calcination to obtain Co_3O_4 nanoparticles [13,14]. Researchers have reported the synthesis of Co_3O_4 nanoparticles from the calcination of $Co_2(OH)_3Cl$ [15–19]. Cobalt hydroxychloride ($Co_2(OH)_3Cl$) belongs to the group of cobalt layered basic salts. Three polymorphs of $Co_2(OH)_3Cl$ have been reported including, the green $Co_2(OH)_3Cl$ [20], the lavender-coloured β-$Co_2(OH)_3Cl$ [21–23] and the pink β-$Co_2(OH)_3Cl$ [24,25]. Among the many uses of $Co_2(OH)_3Cl$ are electrode materials for batteries, electrochemical supercapacitors, microwave absorption and catalysts [26–29].

Studies on nanofluids containing Co_3O_4 nanoparticles dispersed in different heat transfer fluids for potential heat transfer applications have been conducted [30–32]. Nanofluids can be prepared using either a one-step or a two-step approach [33]. The former process involves synthesising and dispersing nanoparticles simultaneously in the base fluid to produce the desired nanofluid. The second process involves synthesising the nanoparticles first and then dispersing them into the base fluid. Previous researchers have studied the thermal conductivity of Co_3O_4-H_2O nanofluids prepared via the two-step method. Among the most influential parameters on thermal conductivity are temperature, particle concentration, particle size and particle shape [34]. The thermal conductivity of Co_3O_4-H_2O nanofluid has been studied by Sekhar et al. [35], Mitra et al. [36], Alsboul et al. [37] and Manoram & Moorthy [38] at various nanoparticles concentration and at constant temperature. Most of the studies evaluated commercial 50 nm Co_3O_4 particles at various concentrations in water to determine which of the thermal conductivities models best describes the resulting thermal conductivities of the nanofluids. According to their results, the addition of Co_3O_4 nanoparticles to water increased the thermal conductivity of nanofluids over that of the base fluid. Additionally, the thermal conductivity enhancement increased with increasing nanoparticle concentration. Temperature dependence of thermal conductivity of Co_3O_4-H_2O nanofluid was investigated by Sekhar et al. [35] at various temperatures (40–60 °C) and various volumetric concentrations (0.1–0.4 vol%). They found that temperature rise led to 25 % increase in thermal conductivity. Mitra et al. [36] synthesised Co_3O_4 to obtain different sizes and shapes to evaluate their effect on thermal conductivity. These Co_3O_4 were synthesised by calcining the cobalt hydroxide precursor at high temperatures (400 °C). Using nanorods with a crystallite size of 27 nm, Mitra et al. [36] prepared rod-based nanofluids, while nanoflowers with a crystallite size of 32 nm were used to prepare flower-based nanofluids. Nanoparticle size, however, was not discussed by the authors as a factor in enhancing thermal conductivity. Furthermore, Mitra et al. [36] reported higher nanofluid thermal conductivity with increasing temperature. They also found that rod-based nanofluids exhibited a 21 % enhancement in thermal conductivity, while flower-based nanofluids only showed a 3 % enhancement. Rod-based nanofluids exhibited enhanced thermal conductivity because of the higher aspect ratios of nanorods [44] leading to an increased contact area with the heat source, and hence increased heat transfer rates [45]. Alsboul et al. [37] reported a 25 % enhancement in thermal conductivity with an increase in temperature. Manoram & Moorthy [38] obtained a 24 % enhancement in thermal conductivity with temperature increment. According to Manoram & Moorthy [38], Brownian motion is the primary mechanism responsible for temperature-induced thermal conductivity enhancement, with micro convection playing an important role as well.

Based on the available literature it is understood that the shape of Co_3O_4 nanoparticles has an impact on the thermal conductivity of their water based nanofluids. This shows that by altering nanoparticles shape, it is possible to enhance their properties for future applications. Nanoparticle size and shape can be controlled by using alcohol during nanoparticle synthesis, since the properties of alcohols change as the alkyl chain length increases [46–48]. In Heuvel et al. [14], a preparation of Co_3O_4 rhombic like particles was carried out by dissolving $CoCl_2.6H_2O$ in different alcohols including methanol, ethanol, propanol, butanol and octanol. They concluded that Co_3O_4 nanoparticle size increases with increasing alcohol concentration. For instance, the size of Co_3O_4 nanoparticles increased from 34 nm to 66 nm with propanol concentration increase from 50 % to 100 %, respectively.

Recently, molecular dynamics (MD) simulations have demonstrated considerable promise in studying nanofluids properties such as thermal conductivity and dynamic viscosity [49,50]. Combining experimental and computational methods has proven effective in enhancing our understanding of nanostructured materials including nanofluids [51,52]. MD simulations involve applying Newton's laws of motion to interacting particles, providing valuable insights into material behaviour at the atomic level. These simulations facilitate the identification, clarification, and investigation of key mechanisms at the nanoscale. Employing force field models, including empirical interatomic potentials, MD simulations calculate exact trajectories of interacting atoms by following their spatial evolution in time. It also predicts and mimics behaviour of molecular systems with great reliability. As a result, researchers often favour MD simulations for investigating the thermophysical properties of materials because of their accuracy and flexibility as a computational tool [53,54].

The impact of the shape and size of Co_3O_4 nanoparticles on the thermal conductivity of their nanofluids was studied. In contrast, no such study has been published on using $Co_2(OH)_3Cl$ without further calcination to eliminate the energy intensive process of transformation to Co_3O_4. In this work, $Co_2(OH)_3Cl$ nanoparticles were therefore synthesised via hydrothermal precipitation at varying concentrations of propanol to explore the influence of propanol concentration on their morphology and size. This strategy allows for changing only one process parameter to achieve various particle shapes and sizes. The propanol can be distilled and reused, making the process environmentally benign. Furthermore, this investigation presents, for the first time, the impact of $Co_2(OH)_3Cl$ nanoparticle size and morphology on the thermal conductivity of water-based nanofluids. To assess the viability of $Co_2(OH)_3Cl$-H_2O as an effective heat transfer medium, thermal conductivity (k) analyses were conducted using a custom-built guarded hotplate apparatus across a temperature range spanning from 298 K to 318 K. Two past studies from Alsboul et al. [37] and Manoram & Moorthy [38] reported theoretical validations for the experimental thermal conductivities values of Co_3O_4-H_2O nanofluids. In contrast, this study presents a computational method using EMD based on the Green-Kubo (EMD-GK) framework employed to obtain the thermal conductivity values that further explain and corroborate the experimental findings.

Experimental methodology

Cobalt hydroxychloride synthesis and characterisation

Chemicals of analytical grade were used without purification in this study. In our experiments, $Co_2(OH)_3Cl$ nanopowders were synthesised using cobalt chloride hexahydrate as a cobalt salt. The cobalt salt was dissolved in mixed propanol/water solvents of different ratios ranging from 0 to 100 %v/v (volume wise) at a molarity of 0.23 M. Ammonium hydroxide solution was added dropwise to adjust the pH of the dissolved solution to ±8.10. The resultant mixture was then transferred to a 0.99 L Teflon-lined pressure reactor equipped with a thermocouple and a self-regulating heating jacket. Following 1 h of ramp-up time, the synthesis was maintained at 105±5 °C for 6 h. Overnight, the pressure reactor was allowed to cool naturally. The resulting green or lavender/pink suspensions were centrifuged, rinsed several times with deionised water (DIW) then with ethanol. Finally, they were dried overnight in an oven at 60 °C.

The nanopowders produced were identified and tested for purity using a Fourier transformed infrared (FTIR) spectrometer equipped with a universal attenuated total reflectance (ATR) accessory (Spectrum two, PerkinElmer, USA) and an X-ray diffractometer (X'Pert Pro, PANalytical, UK). X-Ray diffraction (XRD) analysis was conducted at a voltage and current of 45 kV and 40 mA, respectively. Attenuated total reflectance (ATR)-FTIR spectra of $Co_2(OH)_3Cl$ nanoparticles were collected in the range 4000–400 cm^{-1}. To have a better insight on the morphology of $Co_2(OH)_3Cl$ nanopowders, a JEM-2100 high resolution transmission electron microscope (HRTEM) manufactured by JEOL, Japan, operating at a voltage of 200 kV was used.

Preparation of nanofluids

The $Co_2(OH)_3Cl$ nanopowder samples produced at various propanol concentrations ranging from 0 to 100 % were used to prepare nanofluids via a simple two-step method (Fig. 1). A concentration of 0.03 wt % was maintained for all nanofluids. The weight concentration of $Co_2(OH)_3Cl$ nanofluids was calculated from the weight of $Co_2(OH)_3Cl$ nanopowder and the total weight of the suspension as reported by Li et al. [55]. Following the addition of $Co_2(OH)_3Cl$ nanopowders to DIW, the obtained mixture was sonicated in an ultrasonic bath (240 W) for 4 sessions of 1 h, totalling 4 h and no sedimentation was observed in $Co_2(OH)_3Cl$-H_2O nanofluids as shown in Fig. 2b After sonication, the nanofluids were allowed to cool to ambient temperature before thermal conductivity measurements. The nanofluids remained stable for a maximum of 24 h before sediments formed. The as obtained nanofluids were formulated without adding any surfactant. To guarantee uniformity and stability of the nanoparticles in the base fluid the parameters for sonication time and power of the sonicator (240 W) were kept constant for all the nanofluids measured. Measurements of thermal conductivity were done under 12 h, a time in which the nanoparticles remain suspended in solution. This is based on the fact that sedimentation was observed only after 24 h. Sonication definitely helped in dispersing the nanoparticles in solution by breaking down any possible agglomerates consequently improving on the ability of the nanoparticles to stay suspended in solution during a 24 hour time-frame. Following this two-step preparation of $Co_2(OH)_3Cl$-H_2O nanofluids, their optical analysis was conducted using a UV–VIS-NIR spectrometer (Cintra 2020, GBC, Australia).

Thermal conductivity apparatus description

The thermal conductivity of $Co_2(OH)_3Cl$-H_2O nanofluids was measured using a homemade cylindrical cell apparatus based on the steady-state method as given in a previous study [77]. The apparatus comprises two concentric cylinders made of copper. Using an electric heater, the inner cylinder was heated and kept at the desired temperature (T_h). To change the inner cylinder temperature, the electric power applied to the heater was varied by using a DC power source which allowed to regulate the current with a 0.1 % stability. The outer cylinder was kept at a cold temperature (T_c) by an external supply of cooling water originating from a water bath. During the experiment, heat flows

Fig. 1. $Co_2(OH)_3Cl$-H_2O nanofluid preparation procedure.

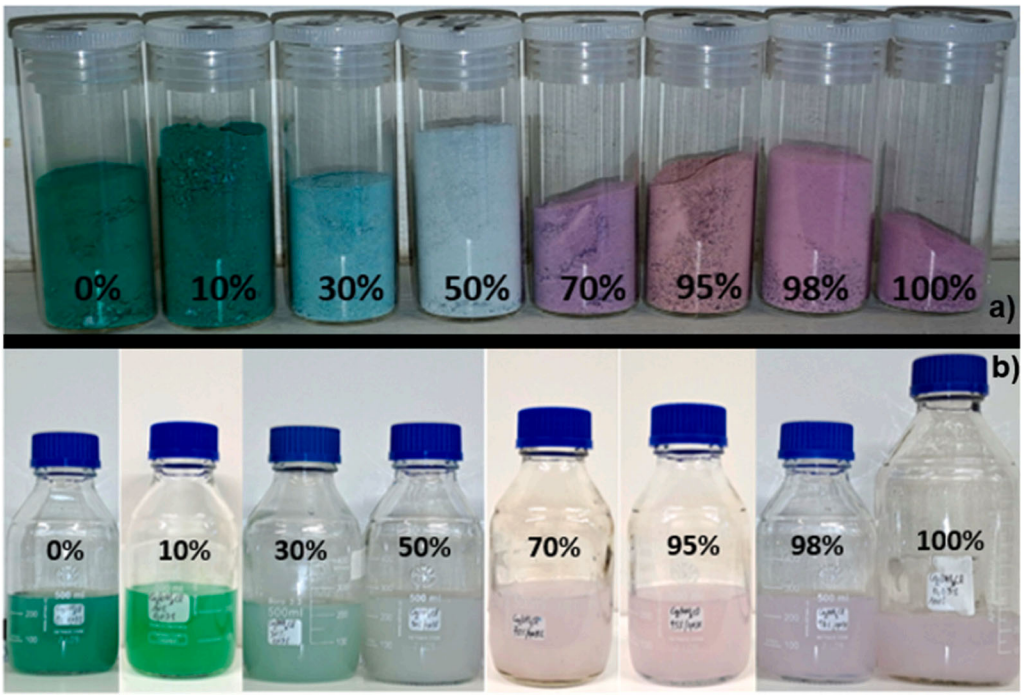

Fig. 2. (a) $Co_2(OH)_3Cl$ nanopowders from propanol concentrations ranging from 0 to 100 % (left to right); (b) $Co_2(OH)_3Cl$-H_2O nanofluids synthesised from different propanol concentrations at 0.03 wt % after 4 h of sonication.

radially from the inner hot cylinder to the outer cold cylinder through the annular space filled with the testing sample ($Co_2(OH)_3Cl$-H_2O nanofluid). To minimise heat loss during the measurements, the cylindrical cell sides were insulated. Temperatures were measured using four calibrated K-type (Copper/Constantan) thermocouples, positioned along the height of the cylinders, from bottom to top, to measure the spatial temperature distribution in both the inner and outer cylinders of the thermal conductivity apparatus. The temperature sensors have an accuracy of ±0.5 °C or ± 0.4 % and were wired to a data acquisition system. The thermal conductivity of nanofluid (k_{nf}) expressed in watt per metre kelvin (W/m.K) was obtained based on the one-dimensional Fourier's equation of heat conduction [51,56]:

$$k_{nf} = \frac{Q\ d}{A\ (T_h - T_c)} \tag{1}$$

Where Q is the heat flow rate ($Q = 1.081$ W), which is equal to the electric power calculated from the measured current ($I = 0.47$ A) and voltage ($U = 2.3$ V) applied to the inner cylinder. The lateral surface area, $A = 2\pi rL$ (in m^2), corresponds to the hot cylinder, with a radius $r = 0.0075$ m and length $L = 0.032$ m. The radius of the outer cylinder was 0.011 m, while its length was similar to that of the inner cylinder. The nanofluid layer thickness, d, between the inner and outer cylinders is 0.0035 m. The temperatures of the inner and outer cylinders, respectively T_h and T_c, were recorded using a Keithley DAQ6510 Data Acquisition System over a temperature range of 298 K to 318 K.

A calibration test involved measuring the thermal conductivity of deionised water, showing a maximum deviation from the reference values of around 2.7 %. Measurements of the thermal conductivity of $Co_2(OH)_3Cl$-H_2O nanofluids at 0.03 wt % but different particle sizes and shapes were taken across a temperature range from 298 to 318 K.

Computational methodology

In MD simulation, atomic motions are governed by Newton's second law, whereas the force exerted on each atom is determined by its position and the associated molecular force fields [57].

MD simulation model and molecular force fields

MD simulations were carried out on three separate systems, each containing identical nanoparticles (i.e., $Co_2(OH)_3Cl$ nanoparticles) with different shapes (i.e., rhombus nanoplates and spherical). These nanoparticles were dispersed in H_2O media to form $Co_2(OH)_3Cl$-H_2O nanofluids, as depicted in Fig. 3. Prior to performing MD simulations, the nanoparticles were created using a molecular editor and visualisation software (i.e., Avogadro). The shape of the nanoparticles was achieved using a tool to convert and manipulate atomic data (i.e., Atomsk). These nanoparticles were then dispersed in water using PACKMOL as a package to create the initial configurations for molecular dynamics simulations (Fig. 3).

Additionally, considering the complex interaction of $Co_2(OH)_3Cl$ nanoparticles in aqueous media, the Universal Force Field (UFF) was employed to describe the atomic interactions of the investigated nanoparticles within the nanofluid. Moreover, the Lennard-Jones (LJ) potential ($V(r_{ij})$) was utilised to model the interatomic interactions among water molecules and other non-bonded interactions in the $Co_2(OH)_3Cl$-H_2O nanofluid system. The LJ potential is expressed in kilojoule per mole (kJ/mol) and its equation is given by [58]:

$$V(r_{ij}) = 4\varepsilon_{ij}\left[\left(\frac{\sigma_{ij}}{r_{ij}}\right)^{12} - \left(\frac{\sigma_{ij}}{r_{ij}}\right)^{6}\right] \tag{2}$$

Here, ε_{ij} is in kJ/mol and it represents the depth of the potential well, σ_{ij} is the finite distance at which the pairwise potential becomes zero, expressed in angstrom (Å), and r_{ij} is also in Å and it indicates the distance between atoms i and j. Moreover, the large-scale atomic/molecular massively parallel simulator (LAMMPS) was utilised for all MD simulations. Firstly, energy minimisation for 4000 steps was performed for the $Co_2(OH)_3Cl$-H_2O nanofluid system followed by equilibration for 200 picoseconds (ps) in the canonical ensemble (NVT) with periodic boundary conditions in a 3D computational domain using the Nose−Hoover thermostat, maintaining conservation of particle number (N), volume (V), and temperature (T). MD simulations were carried out for 200,000 timesteps with a time increment of 0.01 femtoseconds (fs), following equilibrium of the system at a constant temperature and

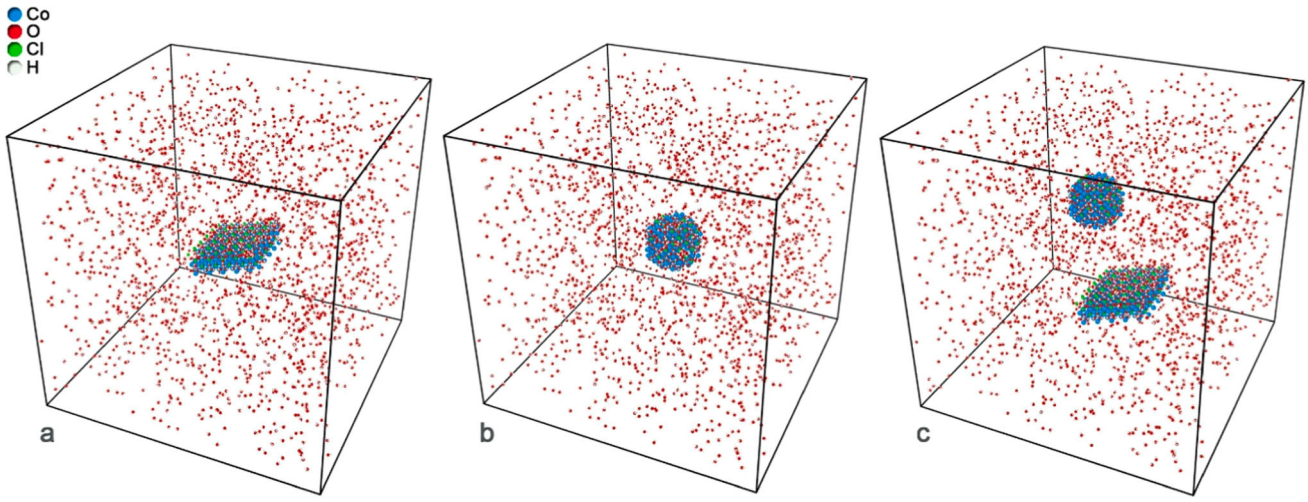

Fig. 3. Initial configuration of $Co_2(OH)_3Cl$-H_2O nanofluids MD models with periodic boundary conditions in a simulation box with dimensions of 150 Å × 150 Å × 150 Å, (a) with $Co_2(OH)_3Cl$ rhombus nanoplates; (b) with $Co_2(OH)_3Cl$ spherical nanoparticle; (c) with both $Co_2(OH)_3Cl$ shapes.

pressure. Usually, each MD result was obtained by conducting four separate simulations and including error estimation.

Integration of EMD-GK for calculating the thermal conductivity

In MD simulations, the Green-Kubo approach uses the linear-response theory and fluctuation-dissipation theorem to describe system dynamics through time autocorrelation functions (ACF) [59]. Moreover, the transport properties of nanofluids are also obtained by integrating the ACF over time in MD simulations, which enables the calculation of thermal conductivity in the equilibrium state [60]. The Green– Kubo formula can be expressed as [61]:

$$k = \frac{1}{3k_B VT^2}\int_0^\infty \left\langle \vec{J_q}(0)\vec{J_q}(t)\right\rangle dt \tag{3}$$

In formula 3, k represents the thermal conductivity in W/m.K, k_B is the Boltzmann constant in joule per kelvin (J/K), V stands for volume in cubic metre (m^3), T is the temperature in K, $\vec{J}_q$ is expressed in watt per square metre (W/m^2), it represents the instantaneous microscopic heat flux vector, and the angular brackets <> signifies the ensemble average. $<\overrightarrow{Jq}(0)\overrightarrow{Jq}(t)>$ refers to the autocorrelation function of microscopic heat flow expressed in square watt per metre to the fourth power (W^2/m^4), and the calculation of the heat flow vector is determined by:

$$\vec{J_q} = \frac{1}{V}\left\{\sum_i E_i\vec{v_i} + \frac{1}{2}\sum_{i<j}\left[\vec{f_{ij}}.(\vec{v_i}+\vec{v_j})\right]\vec{r_{ij}} - \sum_\alpha h_\alpha \sum_i \vec{v_i}\right\} \tag{4}$$

Where $\vec{v}_i$ in metre per second (m/s) represents the velocity of atom i, $\vec{r}_{ij}$ and $\vec{f}_{ij}$ refer to the distance (m) and force in newton (N) vectors connecting atoms i and j, α represents the type of atom in the nanofluid system, and h_α is the enthalpy corresponding to that specific type of atom and is expressed in joule (J). The total energy E_i expressed in J is the sum of kinetic and potential energies and can be written as:

$$E_i = \frac{1}{2}m_i\overrightarrow{v_i^2} + \frac{1}{2}\sum_j \varnothing(\vec{r_{ij}}) \tag{5}$$

Where the interatomic potential energy is represented by $\Phi(\vec{r}_{ij})$ and expressed in J.

Additionally, the enthalpy is subtracted from the heat flux as it represents the energy carried by the mediums, rather than the energy exchanged between them [59]. The enthalpy of atomic species is described as:

$$h_\alpha = \frac{1}{N_\alpha}\sum_{i=1}^{N_\alpha}\left[E_i + \frac{1}{3}\left(m_i\overrightarrow{v_i^2} + \frac{1}{2}\sum_{i=1}^{N_\alpha}\vec{r_{ij}}.\vec{f_{ij}}\right)\right] \tag{6}$$

Where N_α represents the number of atoms belonging to the atomic type α. Babaei et al. [62] demonstrated that the characteristics of multicomponent systems are sensitive to a non-zero h_α, and if not subtracted from the convective heat flux, can reflect in the heat current autocorrelation function (HCACF), ultimately resulting in unusual thermal conductivity values when integrated over time. In addition, the heat flux is determined during every time step (Δt) in the MD simulations. And since the time steps are not continuous, Eq. (3) can be used as a type of summation that can be expressed differently as [63]:

$$k = \frac{\Delta t}{3k_B VT^2}\sum_{m=1}^{M}\frac{1}{N-M}\sum_{n=1}^{N-M}\vec{J}(m+n)\vec{J}(n) \tag{7}$$

Where N represents the total number of simulations timesteps after the system reaches equilibrium, while M indicates the number of timesteps used for calculating the average value of the thermal conductivity (k). The outer summation in Eq.7 denotes the heat-flux autocorrelation function (HFACF).

Results and discussion

Structural and morphological analysis of the synthesised $Co_2(OH)_3Cl$ nanoparticles

The crystalline structure of the synthesised nanoparticles was identified through X-ray diffraction (XRD). Fig. 4 illustrates the diffraction patterns of $Co_2(OH)_3Cl$ nanoparticles synthesised at propanol concentrations ranging from 0 to 100 %v/v. The diffraction peaks observed in most samples were identified and attributed to the standard diffraction data of $Co_2(OH)_3Cl$ (JCPDS card no. 73-2134). The characteristic diffraction peaks of $Co_2(OH)_3Cl$ located at 16.2°, 32.4°, 39.6°, 49.8°, 53.5° and 59.8° were clearly observed in all samples and correspond to the (101), (113), (024), (033), (220) and (208) crystal planes of the $Co_2(OH)_3Cl$ rhombohedral structure, respectively similarly to previous reports [17,19,29]. The nanopowders produced at 70 % and 100 % propanol concentrations showed no additional peaks, indicating their purity. Ma et al. [29] synthesised $Co_2(OH)_3Cl$ by using $CoCl_2.6H_2O$, propylene oxide and an ethanol-water solvent mixture. As a mechanism, they proposed that dissolved $CoCl_2.6H_2O$ exists as an aqueous complex $[Co(H_2O)_6]^{2+}$, a proton-supplying acid, whereas propylene oxide serves as a proton-consuming base [15,29]. The complex $[Co(H_2O)_6]^{2+}$ barely

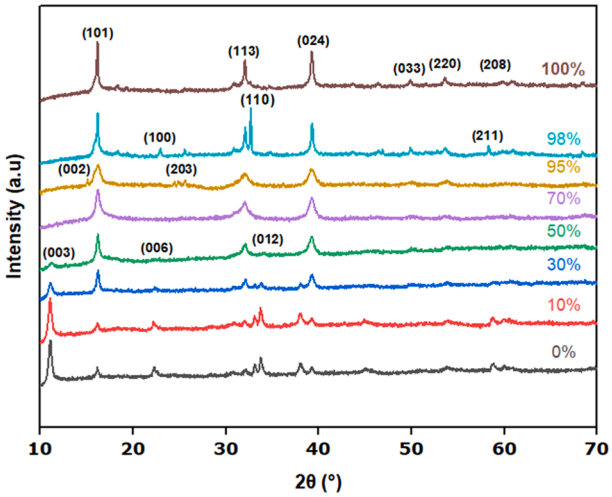

Fig. 4. XRD patterns of $Co_2(OH)_3Cl$ nanopowders synthesised in 0 to 100 % propanol concentration.

hydrolysed because of its low acidity, resulting in Cl^- coordination in the lattice of crystallised species hence producing $Co_2(OH)_3Cl$ [15,29]. The $Co_2(OH)_3Cl$ formed in this study is believed to have been produced via a similar mechanism to that explained above, although an alternate solvent and precipitating agent were used. In the case of the nanopowders produced at 0 %, 10 %, 30 % and 50 % propanol concentration, some peaks were detected at 2θ values of 11.1°, 22.3° and 33.8°, which correspond to the crystal planes of (003), (006) and (012), respectively. Those peaks matched well with the standard card of $Co_{1.176}(OH)_2Cl_{0.348}(H_2O)_{0.456}$ as reported by Ma et al. [64]. The presence of $Co_{1.176}(OH)_2Cl_{0.348}(H_2O)_{0.456}$ can be due to the excess of water molecules. As observed in Fig. 4, the characteristic peaks of $Co_{1.176}(OH)_2Cl_{0.348}(H_2O)_{0.456}$ phase decreased with increasing propanol concentration from 0 to 50 % and eventually disappeared. This indicates that propanol concentration affects the $Co_2(OH)_3Cl$ nanoparticle purity. In the case of nanopowders obtained at 95 % propanol concentration, some minor peaks were observed at 15.1° and 25.5° which correspond to the (002) and (203) crystal planes of cobalt ammine chloride (JCPDS card no. 70-0787), as reported by Zhao et al. [65]. In contrast, the nanopowders obtained in 98 % propanol concentration exhibited minor peaks at 22.9°, 32.7° and 58.3° which were assigned to the (100), (110) and (211) crystal planes of salammoniac (JCPDS card no. 07-0007), as previously reported by Zhang et al. [66]. These peaks could be the result of residues of the precipitating agent (NH_4OH) present in the samples

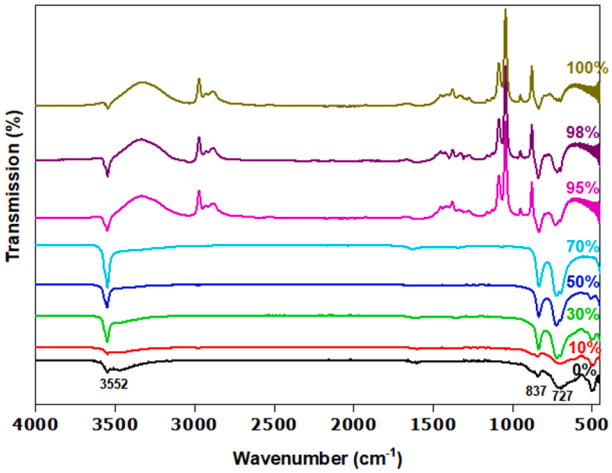

Fig. 5. ATR-FTIR spectra of all $Co_2(OH)_3Cl$ nanopowders.

following synthesis.

Fig. 5 represents the ATR-FTIR spectra of as-prepared $Co_2(OH)_3Cl$ nanopowders where the narrow peak appearing at about 3552 cm^{-1} is attributed to the stretching vibration of O—H as reported in previous works [17,29]. The O—H stretching vibration comes from the chemical structure of $Co_2(OH)_3Cl$ where three separate OH^- group donors are attached to one proton acceptor Cl^-via trimeric or threefold hydrogen bonds [29,67]. In addition, the Co-O stretching vibrations are observed at about 837 and 727 cm^{-1} which were also reported in previous works [17]. The Co-O stretching vibration is due to the crystal structure of $Co_2(OH)_3Cl$ where every OH group is attached to three Co^{2+}ions but has two different Co–O distances: d (Co^K –O) = 2.078 Å and d (Co^T –O) = 2.106 Å [29,68,69].

A change in propanol concentration affected the colour, shape and size of $Co_2(OH)_3Cl$ nanopowders. Fig. 2a displays the $Co_2(OH)_3Cl$ nanopowders of various colours obtained from varying propanol concentrations. Using 0, 10, 30 and 50 % propanol concentrations, various shades of green nanopowders were obtained, similar to that reported by Feitknecht and Fischer [20]. At 70 % and 100 % propanol concentration, lavender nanopowders were produced indicating that the polymorph obtained was the β-$Co_2(OH)_3Cl$ [21–23]. Using 95 and 98 % propanol concentrations, different shades of pink nanopowders were obtained indicating that the polymorph obtained was the β-$Co_2(OH)_3Cl$ similarly to that reported by García-Martínez et al. [24].

Fig. 6 illustrates the shape evolution of different $Co_2(OH)_3Cl$ nanoparticles as a function of propanol concentration. Fig. 6a shows large hexagonal $Co_2(OH)_3Cl$ nanoplates formed in the absence of propanol. The nanopowders produced from 10 % propanol concentration also displayed the same shape (Fig. 6b). However, 30 % and 50 % propanol concentration resulted in size reduction with severe aggregation of the nanoplates (Fig. 6c & Fig. 6d). At a 70 % propanol concentration, the nanoplates lost their hexagonal shape, resulting in spherical as well as irregularly shaped aggregated particles, as shown in Fig. 6e. At 95 % propanol concentration, only $Co_2(OH)_3Cl$ spherical nanoparticles and nanoplates (Fig. 6f) were observed. Furthermore, spherical nanoparticles and rhombus nanoplates along with some clusters and a few large plates (Fig. 6 g, Fig. 6h, Fig. 7a and Fig. 7b) were observed in 98 % and 100 % propanol concentrations. The contribution of these large clusters/plates is trivial, as they tend to precipitate easily due to gravitational effects during measurements, especially when using a less viscous medium such as water. Previous authors reported the synthesis of $Co_2(OH)_3Cl$ hexagonal plates from the dissolution of $CoCl_2$ or $CoCl_2.6H_2O$ in aqueous or ethanol-water in the presence of NaOH or propylene oxide, respectively [18,29]. According to its composition, $Co_2(OH)_3Cl$ is a solid solution of $Co(OH)_2$ and $CoCl_2$ [70]. Furthermore, the layered structured $Co(OH)_2$ often form hexagonal plate-like particles [71]. It is therefore likely that the $Co(OH)_2$ layered structure played a role in the formation of $Co_2(OH)_3Cl$ hexagonal nanoplates at low propanol concentrations, as reported in this study.

The particle size of each sample was obtained from the TEM images (Fig. 6), by measuring 200 particles using the Feret diameter tool of the ImageJ software. Only 35 nanoparticles were measured for the nanopowders obtained at 0 %, 10 %, 30 %, and 50 % propanol concentrations due to the type of images obtained. Based on the norm, it is required to measure at least 200 nanoparticles, so it was necessary to test the validity of using 35 nanoparticles for particle size distribution. A total of 35 nanoparticles were randomly measured from the $Co_2(OH)_3Cl$ nanoparticles in 70 %, 95 %, 98 % and 100 % propanol concentration to perform the evaluation. A comparison was made between the averages and standard deviations of 35 nanoparticles samples and those obtained from the 200 nanoparticles initially measured. Comparing the averages from 35 and those of 200 measurements for the same samples, they showed differences of 13 %, 16 %, 2 %, 2 % for $Co_2(OH)_3Cl$ synthesised at 70 %, 95 %, 98 % and 100 % propanol concentrations, respectively. Due to these minimal variations, the results for the 35 nanoparticles from 0 %, 10 %, 30 % and 50 % propanol concentration are presented as

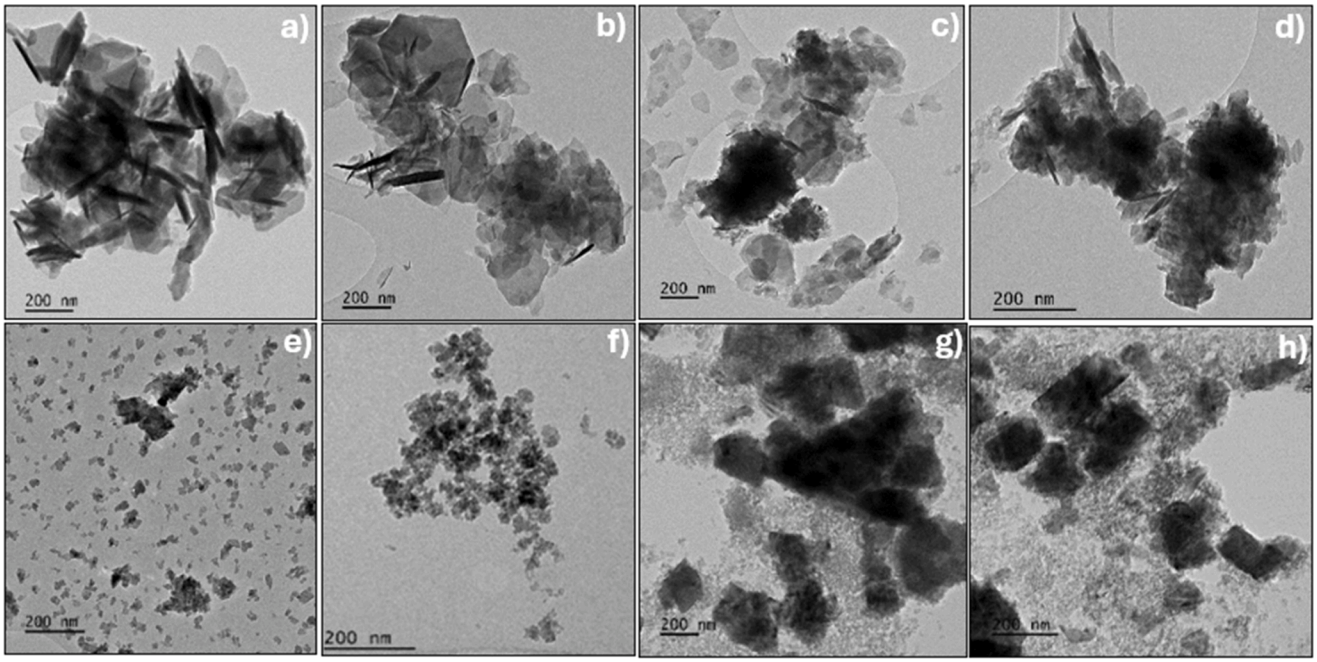

Fig. 6. TEM images of $Co_2(OH)_3Cl$ nanoparticles in 0 to 100 % propanol concentrations.

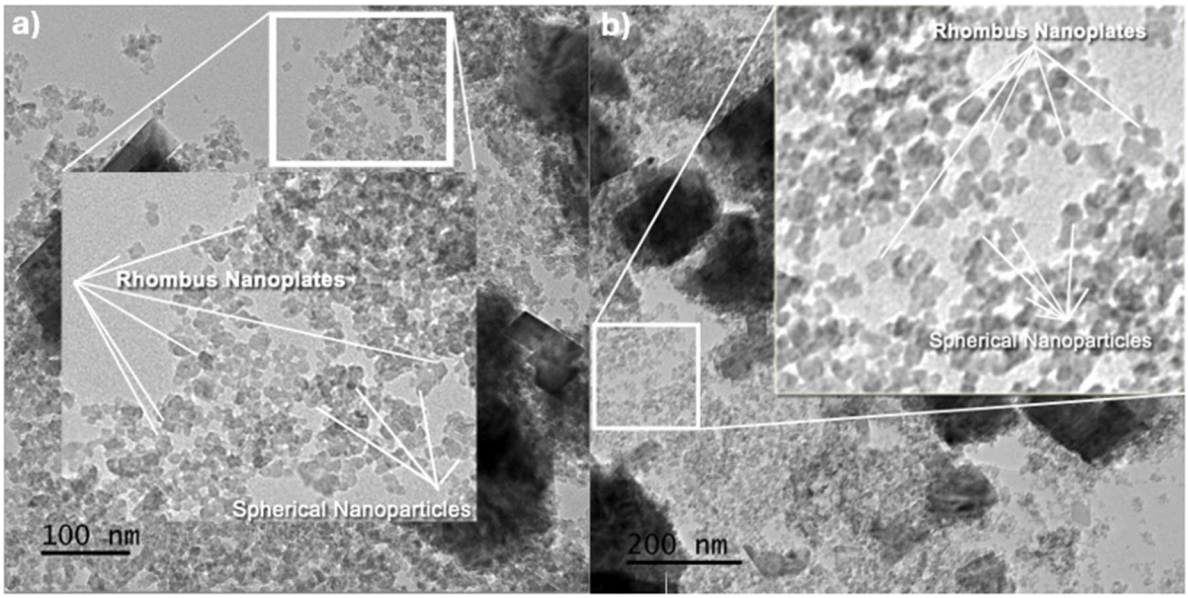

Fig. 7. (a) TEM image of $Co_2(OH)_3Cl$ nanoparticles produced at 98 % propanol (the inset shows the high-resolution TEM images of $Co_2(OH)_3Cl$ spherical nanoparticles and rhombus nanoplates); (b) TEM image of $Co_2(OH)_3Cl$ nanoparticles produced at 100 % propanol (the inset shows the high-resolution TEM images of $Co_2(OH)_3Cl$ spherical nanoparticles and rhombus nanoplates).

representative. Consequently, 35 nanoparticles were measured from each sample to determine the average diameter of the synthesised $Co_2(OH)_3Cl$ nanomaterials, with the Feret particle diameter being specifically determined using the ImageJ program for each batch of images. A summary on the average sizes and other characteristics of as-synthesised $Co_2(OH)_3Cl$ nanoparticles is presented in Table 1.

Fig. 8 shows the size distribution curves of $Co_2(OH)_3Cl$ nanoparticles at different propanol concentrations. The $Co_2(OH)_3Cl$ nanoparticles synthesised at propanol concentrations ranging from 0 to 50 % displayed larger sizes ranging from 83.7 nm to 56.1 nm (Fig. 8a to Fig. 8d) in comparison to $Co_2(OH)_3Cl$ nanoparticles obtained at propanol concentrations ranging from 70 to 100 %, which showed smaller sizes ranging from 22.6 nm to 9.6 nm (Fig. 8e to Fig. 8h). It is clear that both the average size and size distribution curves of $Co_2(OH)_3Cl$ nanoparticles are affected by the change in propanol concentration. For instance, at 50 % propanol concentration, the size of the $Co_2(OH)_3Cl$ particles was reduced by 33 % as opposed to when no propanol was used. Due to the lack of previous studies reporting the effect of propanol on the synthesis of $Co_2(OH)_3Cl$ nanoparticles, a direct comparison regarding the nucleation and growth of $Co_2(OH)_3Cl$ nanoparticles in propanol could not be established. The trend obtained in this study is opposed to that reported by Heuvel et al. [14], who found that the size of Co_3O_4 nanoparticles increased from 34 nm to 66 nm with an increment in propanol concentration from 50 % to 100 %. However, the trend

Table 1
Size, shape, colour, and phases of $Co_2(OH)_3CI$ nanoparticles obtained at different propanol concentrations.

Propanol concentration (%)	Average size (nm)	Shape (predominant structures)	Colour	Phase
0	83.7 ± 4.2	Large hexagonal nanoplatelets	Dark green	α – phase
10	57.7 ± 2.1	Hexagonal nanoplatelets	Dark green	α – phase
30	57.7 ± 1.9	Nanoplatelet aggregation	Blue-green (lighter green)	α – phase
50	56.1 ± 3.4	Nanoplatelet aggregation	Even lighter green	α – phase
70	22.6 ± 0.5	Spherical nanoparticles Irregular shapes	Lavender	β – phase
95	11.7 ± 2.5	Spherical nanoparticles + nanoplatelets	Pink	β – phase
98	11.0 ± 0.4	Spherical nanoparticles + rhombus nanoplatelets Aggregation	Pink/ Lavender	β – phase
100	9.6 ± 0.1	Spherical nanoparticles + rhombus nanoplatelets Irregular shapes Aggregation	Lavender	β – phase

observed in this study is similar to the results of Chowdhury et al. [72], who found that increasing the amount of propanol inhibited the growth of akaganeite (β-FeOOH) nanorods transversally and longitudinally.

Optical analysis of $Co_2(OH)_3Cl$ nanofluids

The transmittance spectrum for both water and $Co_2(OH)_3Cl$-H_2O nanofluids at 0.03 wt % are presented in Fig. 9. In the near infrared region, both water and $Co_2(OH)_3Cl$ nanofluids showed absorption peaks (1149 nm and 972 nm). $Co_2(OH)_3Cl$ nanofluids exhibit a decrease in transmittance at 1149 nm, as their transmittance drops from ~43 % to 27 % as propanol concentration increases from 0 to 100 %. A decrease in $Co_2(OH)_3Cl$ nanofluid transmittance from ~64 % to 34 % at 972 nm with increasing propanol content can be observed. As seen from Fig. 9, water showed high transparency (~88 % transmittance) in the visible spectrum whereas all $Co_2(OH)_3Cl$ nanofluids exhibited better absorbency in the visible spectrum (400–700 nm), indicating their capability to absorb visible light.

Thermal conductivity of $Co_2(OH)_3Cl$ nanofluids: experimental investigations

In this section, the temperature-dependent thermal conductivity of different $Co_2(OH)_3Cl$-H_2O nanofluids is shown in Fig. 10. The $Co_2(OH)_3Cl$-H_2O nanofluids displayed higher thermal conductivity than those of pure water. The thermal conductivity of nanofluids increased with increasing temperature and decreased particle size. As shown in Fig. 10, the nanofluids containing hexagonal $Co_2(OH)_3Cl$ nanoplates with sizes ranging from 83.7 nm to 56.1 nm exhibited lower thermal conductivity than those made of $Co_2(OH)_3Cl$ nanospheres and rhombus nanoplates with sizes ranging from 22.6 nm to 9.6 nm. Studies have reported that the use of narrow sized nanoparticles (SiC, ZnO, TiO_2) with a higher surface area to volume ratio led to higher thermal conductivity of the resultant nanofluids [73–76]. Despite the larger surface area of the hexagonal plate-like $Co_2(OH)_3Cl$ particles, they displayed lower thermal conductivity enhancement which could be due to their larger lateral dimensions which could lead to agglomeration and

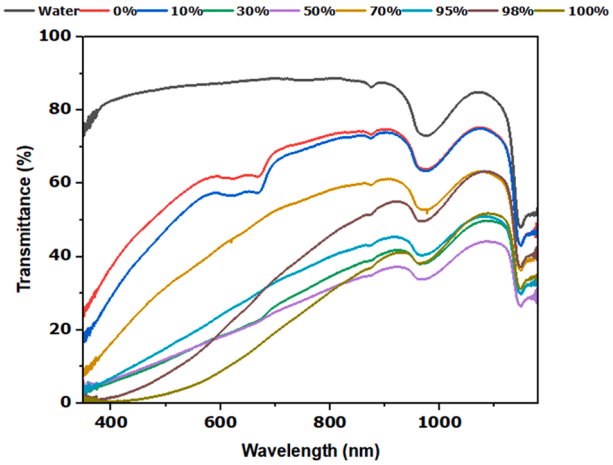

Fig. 9. UV–VIS-NIR spectrum of $Co_2(OH)_3Cl$ nanofluids issued from different propanol concentrations.

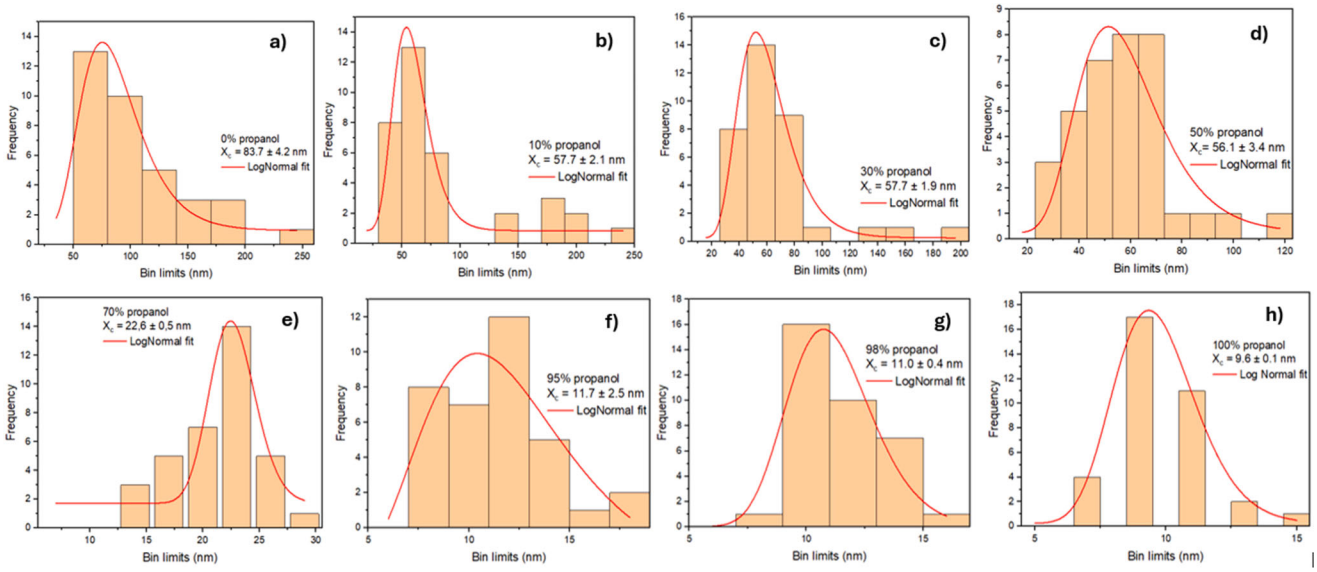

Fig. 8. Particle size distribution curves of $Co_2(OH)_3Cl$ nanoparticles.

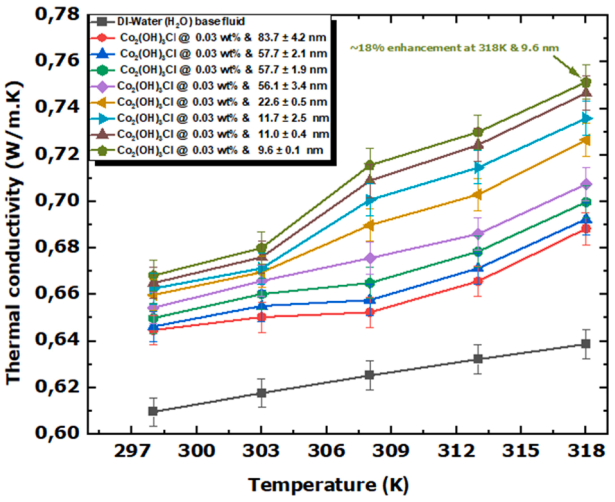

Fig. 10. Thermal conductivity of $Co_2(OH)_3Cl$-H_2O nanofluids at different temperatures. Error bars represent 2.7 % uncertainty in the reported data.

sedimentation. It is thought that the particle size and shape played a greater role on the enhanced thermal conductivity of $Co_2(OH)_3Cl$-H_2O nanofluids which can explain the trend observed in this study. Fig. 11 shows the effect of $Co_2(OH)_3Cl$ particle size on the thermal conductivity enhancement of their aqueous nanofluids. The addition of $Co_2(OH)_3Cl$ nanoparticles at 9.6 nm to water resulted in raising the thermal conductivity of $Co_2(OH)_3Cl$-H_2O nanofluid from 9.6 % to 14.5 % from 298 K to 308 K compared to pure water. When the temperature increased from 308 K to 318 K, the thermal conductivity of $Co_2(OH)_3Cl$-H_2O nanofluid increased from 14.5 % to 17.7 %. The highest enhancement in thermal conductivity corresponds to the temperature of 318 K for all $Co_2(OH)_3Cl$ nanofluids. This aspect of the study shows that reducing particle size from 84 nm to ~10 nm results in a clear increase in thermal conductivity enhancement. Three mechanisms that could explain the enhanced thermal conductivity of nanofluids include the clustering of nanoparticles, the liquid nanolayer formation over the nanoparticles, and the Brownian motion of nanoparticles [31,32,38,77,78]. When the Van der Waals attraction force exceeds the repulsive force, the nanoparticles tend to aggregate and results in clusters formation within the base fluid [79]. Clusters of nanoparticles could create paths facilitating the conduction of heat, which may contribute to enhancing the thermal

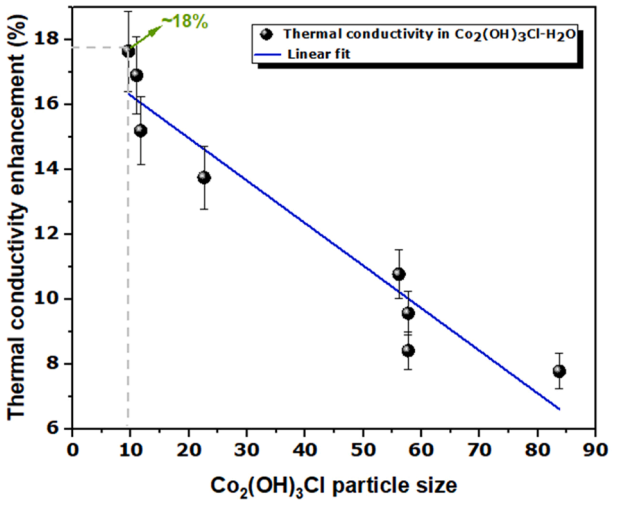

Fig. 11. Thermal conductivity enhancement of $Co_2(OH)_3Cl$ nanofluids at various particle sizes. Error bars represent 2.7 % uncertainty in the reported data.

conductivity of nanofluids [80]. The layering of liquid molecules at the surface of nanoparticles can also enhance the thermal conductivity of nanofluids [81]. Liquid molecules layering provides a thermal bridge between the nanoparticles and the dispersing fluid, leading to efficient thermal transport [81]. The Brownian motion of dispersed nanoparticles is considered to be a major factor in explaining both particle size and temperature-dependent thermal conductivity of nanofluids [32,82]. Brownian motion is caused by the collision between nanoparticles and that between the base fluid molecules and the nanoparticles. Collisions between nanoparticles facilitate energy transfer between them. As temperature rises, $Co_2(OH)_3Cl$ nanoparticles gain kinetic energy and move faster. As $Co_2(OH)_3Cl$ nanoparticles are more intensely motioned, the Brownian motion-induced convection and contributes more to heat transport, enhancing the thermal conductivity of the resulting nanofluids as reported by different researchers [81,83]. The smallest size (9.6 nm) of $Co_2(OH)_3Cl$ nanoparticles was formed at 100 % propanol concentration. According to the Brownian theory, the smaller the colloid particle size, the faster it moves, resulting in increased heat transfer inside the fluid [84]. This could also lead to a significant increase in collisions between smaller $Co_2(OH)_3Cl$ nanoparticles and water molecules, which will further enhance the thermal conductivity. Past studies have reported similar trends about the role of particle size on the thermal conductivity enhancement of water-based nanofluids. For instance, alumina nanofluids displayed enhanced thermal conductivity with decreasing particle size at 283 K, 303 K and 323 K [85] and in a temperature range of 283 K - 353 K [86].

From the above results, the dispersion of as-synthesised $Co_2(OH)_3Cl$ dried at 60 °C in an oven to water can produce nanofluids that yield similar thermal conductivity performances as observed with Co_3O_4 generally obtained through annealing hydrothermally synthesised cobalt-precursors. For instance, the Co_3O_4-H_2O nanofluid from Alsboul et al. [37] showed an increase in thermal conductivity from 0.630 to 0.666 W/m.K at 0.05 wt % and a particle size $\leq$ 50 nm, while in this study, the thermal conductivity of $Co_2(OH)_3Cl$-H_2O nanofluid increased from 0.668 to 0.751 W/m.K at 0.03 wt % and a particle size $<$ 10 nm, from 298 K to 318 K. At 318 K, our thermal conductivity improvement was roughly three times better than that of Alsboul et al. [37]. It is likely that carrying out thermal conductivity measurements of $Co_2(OH)_3Cl$-H_2O nanofluids with particle sizes below 10 nm at 60 °C, 70 °C instead of 45 °C down to 25 °C as done in this study will produce similar thermal conductivity enhancements as observed by the other 4 researchers who reported thermal conductivity enhancements for Co_3O_4—H_2O nanofluids (Table 2), and perhaps even greater.

The thermal conductivity enhancement value of $Co_2(OH)_3Cl$-H_2O nanofluids at 45 °C is also compared with those from literature reporting thermal conductivity enhancements for CNT-H_2O nanofluids at different temperatures as shown in Table 2. As can be seen, most of the CNT-H_2O nanofluids displayed higher thermal conductivity enhancements due to the good dispersion of CNT in water achieved either via chemical functionalisation or surfactant addition. The surfactant-free $Co_2(OH)_3Cl$-H_2O nanofluid with particle sizes below 10 nm produced in this study displayed 17.7 % thermal conductivity enhancement at 45 °C down to 25 °C. The addition of the required surfactant to $Co_2(OH)_3Cl$-H_2O nanofluids with particle sizes below 10 nm may not only improve nanofluid stability but could also result in higher thermal conductivity improvements than those observed at the same temperature for CNT-H_2O nanofluids. In addition, a comparison was established between the thermal conductivity enhancement obtained in this study at 45 °C and those obtained for CNT-H_2O nanofluids reported by Phuoc et al. [39], Garg et al. [40] and Xing et al. [41] at different temperatures as shown in Fig. 12. It can be seen that an increment in particle concentration (wt %) results in reducing the nanofluid thermal conductivity. Further insight into the mechanisms contributing to the achieved higher thermal conductivity enhancement (17.7 %) of the synthesised $Co_2(OH)_3Cl$-H_2O nanofluid with particle sizes below 10 nm is provided in the next section using molecular dynamics simulations.

Table 2
Comparison of size, shape, nanofluid concentration, thermal conductivity enhancement and temperatures for $Co_2(OH)_3Cl$-H_2O nanofluids prepared in this work versus Co_3O_4 and CNT nanofluids prepared in some previous studies.

Reference	Preparation method & surfactant	Nanoparticle size & shape	Concentration	Temperature	Theoretical validation	TC ratio enhancement	TC enhancement
Sekhar et al. [35] Co_3O_4-H_2O nanofluid	Two step & commercial powder Decyl glucoside	-	0.40 vol%	60°C	No	25%	-
Mitra et al. [36] Co_3O_4-H_2O nanofluid	Two step & hydrothermal synthesis	D = 27 nm (rods) D = 32 nm (flowers)	0.011 wt%	60°C	No	-	21% (rods) 3% (flowers)
Alsboul et al. [37] Co_3O_4-H_2O nanofluid	Two step & commercial powder	D (50 nm)	0.40 wt%	60°C	Yes	-	25%
Manoram & Moorthy [38] Co_3O_4-H_2O nanofluid	Two step & commercial powder CTAB	D (50 nm) (spherical)	0.40 vol%	70°C	No	-	24%
Phuoc et al. [39] MWCNT-H_2O nanofluid	Two step & commercial powder Chitosan	OD (20-30 nm) L (10-30 μm) Tubes	3.0 wt%	25°C	Yes	-	13%
Garg et al. [40] MWCNT-H_2O nanofluid	Two step & commercial powder Gum arabic	OD (10-20 nm) L (0.5-40 μm) Tubes	1.0 wt%	35°C	No	-	20%
Xing et al. [41] SWCNT-H_2O nanofluid	Two step & commercial powder CTAB	OD = 1-2 nm L = 5-30 μm Tubes	1.0 wt%	60°C	No	-	16.2%
Karami et al. [42] Functionalised CNT-H_2O nanofluid	Two step & commercial powder	D (10 nm) L (5-10 μm) Tubes	0.015 vol%	60°C	No	-	27.2%
Assael et al. [43] MWCNT-H_2O nanofluid	Two step & commercial powder SDS	OD (100 nm) L (>50 μm) Tubes	0.6 vol%	25°C	No	-	38%
This work $Co_2(OH)_3Cl$-H_2O nanofluid	Two step & hydrothermal synthesis	<10 nm Rhombus + spherical nanoplatelets	0.03 wt%	45°C	No	-	18%

Thermal conductivity of $Co_2(OH)_3Cl$-H_2O nanofluids: molecular dynamics investigations

$Co_2(OH)_3Cl$ nanoparticles and water radial distribution functions (RDF)

To ensure precision in our molecular dynamics (MD) simulations, we employed a united atomic model to construct the $Co_2(OH)_3Cl$-H_2O nanofluids system. Fig. 13a, b, and c show the radial distribution functions (RDFs) for the rhombus $Co_2(OH)_3Cl$ nanoplates, $Co_2(OH)_3Cl$ spherical nanoparticle, and H_2O base fluid at $T = 298$ K. As expected, the RDF results confirmed the existence of solid $Co_2(OH)_3Cl$ nanoparticles and liquid H_2O in the MD simulation models. The structure of solid $Co_2(OH)_3Cl$ (i.e., Rhombus nanoplates and spherical nanoparticle) has consistent, periodic patterns, with peaks appearing slightly broader due to vibrations of $Co_2(OH)_3Cl$ atoms within their lattice positions. Regarding H_2O base-fluid, RDFs were computed using H and O as shown in Fig. 13c. Based on the results of the radial distribution functions for H—H, O—O, and O—H derived from the H_2O model, distinct initial peaks were observed suggesting its first coordination sphere as a liquid. Furthermore, the inset in Fig. 13c shows that in liquid state, H_2O does not have a consistent molecular structure but instead loses its long-range atomic ordering. The H_2O molecules become decoupled from one another, and the radial distribution function returns to the bulk density, where $g(r) = 1$, confirming the liquid state of the employed H_2O model [87].

Validation of the EMD-GK method for studying the thermal conductivity of pure H2O base fluid

The EMD-GK method was employed to determine the thermal conductivity of H_2O base-fluid as a single-phase within a simulation box containing 6000 molecules under a temperature of 298 K and pressure of 1 atm. The obtained results were compared with existing numerical and experimental data from the literature to validate the EMD-GK simulation method. By using Eq. (7), the base fluid (i.e., H_2O) thermal conductivity (k) was estimated with an acceptable margin of error (±0.02). Nevertheless, it is important to examine the area below the HFACF as it converges over time (see Fig. 14). To ensure accuracy in EMD-GK calculations, it is essential that the HFACF decays to zero within the integral time length [88].

Based on Fig. 14, the HFACF for water decayed monotonically, taking approximately 6000 fs to reach zero at a temperature of 298 K. This finding indicates that the heat flux fluctuations in the water system were damped progressively, resulting in good integral of the HFACF. Furthermore, the consistent oscillations of the HFACF even after 6000 fs correlation time could be due to the unrestricted motion of H_2O molecules, which exhibit strong cohesion across various degrees of freedom such as rotational, translational and vibrational [89].

The average k of the base-fluid (H_2O) was calculated based on the integrands between 6000 and 120,000 fs with smaller HFACF oscillations. k was determined by averaging four independent MD simulation runs of the H_2O system. Each run's deviation was under ±0.005 W/m.K and the deviation of four separate runs was under ±0.006 W/m.K. The result achieved was $k \sim 0.62$ W/m.K at $T = 298$ K, which is in alignment with several numerical simulation findings [90,91], and the experimental value of 0.61 W/m.K obtained for H_2O as the base-fluid in this work as showed in Fig. 15. These findings validated the appropriateness of utilising the EMD-GK method for predicting and examining thermo-physical properties in complex systems like $Co_2(OH)_3Cl$-H_2O nanofluid. The convergence and residual error table (Table 3) is presented below.

Comparative analysis of molecular dynamics (MD) simulations with experimental thermal conductivity for $Co_2(OH)_3Cl$-H_2O nanofluid system

In this study, molecular dynamics (MD) simulations were employed to explore how the shapes of $Co_2(OH)_3Cl$ nanoparticles (i.e., rhombus nanoplates and spherical) affect the thermal conductivity (k) of $Co_2(OH)_3Cl$-H_2O nanofluids with nanoparticle sizes below 10 nm. This investigation was initiated by the experimental observation of a significant enhancement, reaching 17.7 %, in samples containing $Co_2(OH)_3Cl$ nanoparticles with an average size of 9.6 nm. The experimental data obtained were compared with the computationally calculated k values over a temperature range from 298 to 318 K, as shown in Fig. 16. These results revealed a linear increase in thermal conductivity (k) with rising temperatures for the base-fluid and nanofluid. The trends observed in the experimentally measured values closely resemble those predicted by the MD simulations via the EMD-GK method. However, the MD results obtained clearly demonstrate that rhombus $Co_2(OH)_3Cl$ nanoplates with sizes below 10 nm contributed to higher thermal conductivities compared to spherical nanoparticles. Moreover, employing a mixed configuration of both shapes enables more accurate calculations of the

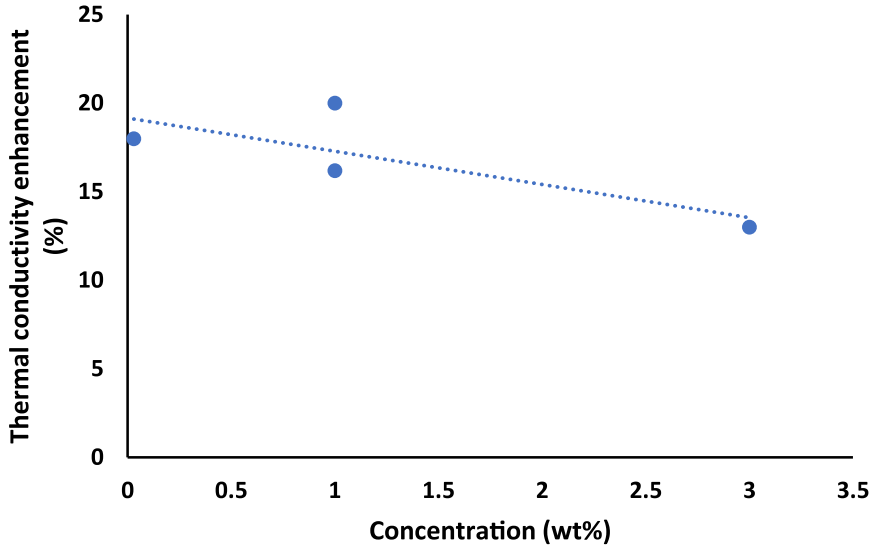

Fig. 12. Comparison of thermal conductivity enhancement of CNT-H_2O and $Co_2(OH)_3Cl$-H_2O nanofluids.

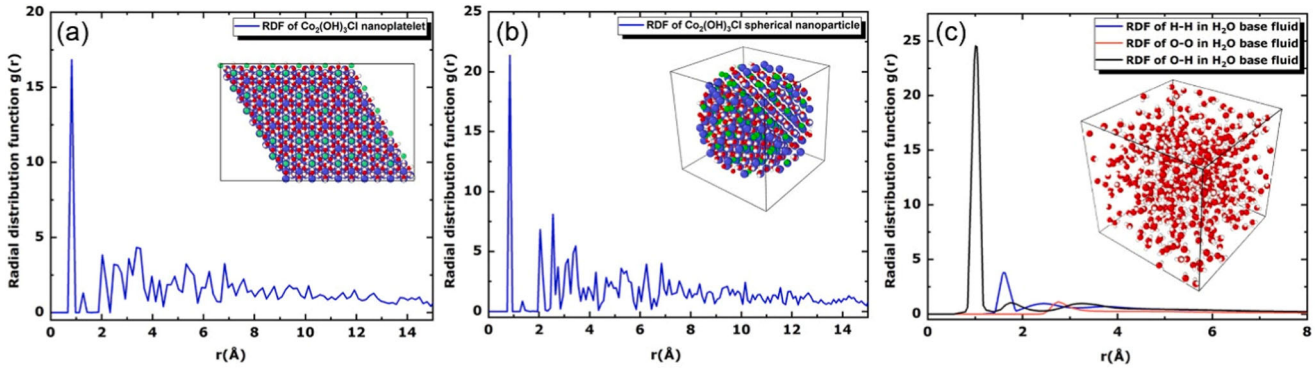

Fig. 13. Radial distribution functions (RDFs) for (a) rhombus $Co_2(OH)_3Cl$ nanoplate; (b) $Co_2(OH)_3Cl$ spherical nanoparticle (c) H_2O base fluid (inset: H_2O MD model).

thermal conductivity of $Co_2(OH)_3Cl$-H_2O nanofluids, especially at higher temperatures. The reason for this phenomenon is likely diffusive heat conduction being more prominent in nanofluids made of rhombus $Co_2(OH)_3Cl$ nanoplates, while the enhancement of thermal conductivity in nanofluids with $Co_2(OH)_3Cl$ spherical nanoparticles is mostly caused by the particles' Brownian motion. It is well-established that the diffusive heat conduction mechanism becomes more effective as the aspect ratio of nanomaterials increases [92,93]. In nanofluids, heat diffusion is generally influenced by the interfacial thermal resistance (ITR), which impedes heat transfer due to interactions between the solid and liquid phases [94,95]. As the temperature increases, the ITR values decrease, resulting in increased heat transfer through thermal diffusion. Consequently, there is an increase in diffusive heat conduction in nanofluids containing $Co_2(OH)_3Cl$ nanoplates. In addition, for nanofluids with spherical nanoparticles, the presence of a long-time tail in Brownian motion significantly impacts the relaxation time of nanoparticles [94]. This tail is due to the hydrodynamic interactions of the moving nanoparticles [96], causing them to require additional time to adjust their motion between consecutive collisions. Consequently, the individual contribution attributed to Brownian motion is reduced significantly. Yet, as the temperature rises, the agitation of nanoparticles also increases, resulting in an enhancement of the Brownian motion of nanoparticles [97]. The larger contact area with the base fluid provided by rhombus $Co_2(OH)_3Cl$ nanoplates, because of their higher surface area-to-volume ratio, contributes to their enhanced heat conductivity compared to spherical nanoparticles [78]. Furthermore, the slight differences in the k numerical and experimental values may be due to the varying sizes and shapes of $Co_2(OH)_3Cl$ nanoparticles observed in the TEM micro-images (Fig. 6h) compared to those modelled in the MD simulation (shown in

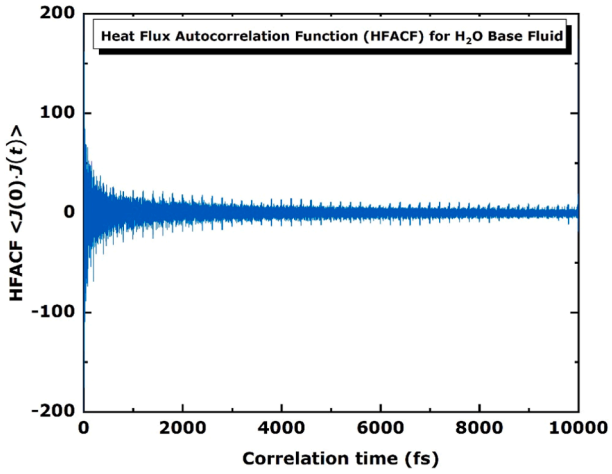

Fig. 14. Computed heat flux autocorrelation functions for H_2O base fluid at $T =$ 298 K and $P =$ 1atm.

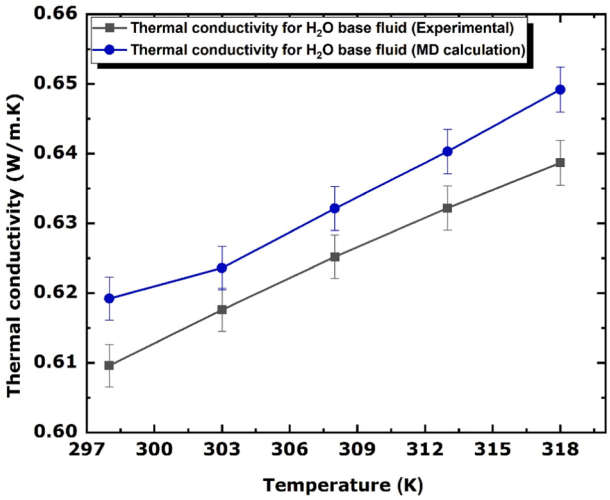

Fig. 15. Measured and computed thermal conductivities of H_2O base-fluid at different temperatures. Error bars represent 2.0 % uncertainty in the reported data.

Table 3
Convergence and residual error table.

Iteration No.	Time Step (fs)	Number of Particles	Thermal Conductivity (W/m·K)	Residual Error	Convergence
1	0.1	18,000	0.617	−0.003	Yes
2	0.5	18,000	0.619	−0.001	Yes
3	0.8	18,000	0.621	+0.001	Yes
4	1.0	18,000	0.623	+0.003	Yes

the inset of Fig. 13a and b). This may result in a discrepancy between the experimental and numerical results [52,98]. Additionally, other potential contributing factors within the synthesis process of $Co_2(OH)_3Cl$-H_2O nanofluid could contribute to these slight discrepancies, such as defects arising in the synthesised $Co_2(OH)_3Cl$. In the present work, these variables were not considered in the thermal conductivity MD calculations. Nevertheless, numerical data for the thermal conductivity of the $Co_2(OH)_3Cl$-H_2O nanofluid match well with experimental results, especially for samples with $Co_2(OH)_3Cl$ nanoparticles smaller than 10 nm.

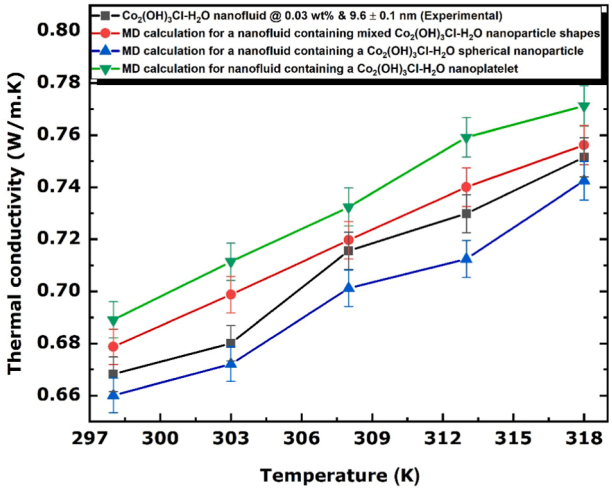

Fig. 16. Measured and computed thermal conductivities of $Co_2(OH)_3Cl$-H_2O nanofluids at different temperatures. Error bars represent 2.0 % uncertainty in the reported data.

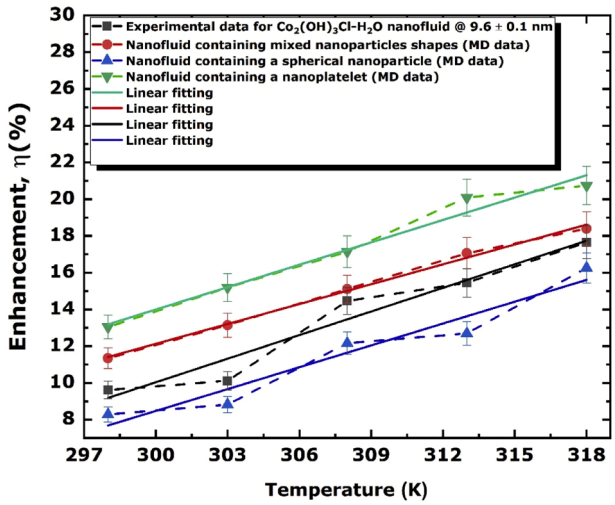

Fig. 17. Relative enhancements η(%) of $Co_2(OH)_3Cl$-H_2O nanofluids at different temperatures Error bars represent 0.5 % percent error of data. Error bars represent 2.0 % uncertainty in the reported data.

Thermal conductivity enhancement, denoted as η(%), is expressed as the percentage variation in the nanofluids (k_{nf}) thermal conductivity compared to the base fluid (k_b). This can be computed via the equation provided below:

$$\eta(\%) = \frac{(k_{nf} - k_{bf})}{k_{bf}} \times 100 \quad (8)$$

The relative enhancements (η) in the thermal conductivity percentage of $Co_2(OH)_3Cl$-H_2O nanofluid synthesised at 100 % propanol and having nanoparticles with a size below 10 nm was calculated by eq. (8) and plotted as a function of temperature (Fig. 17). The average enhancement at 318 K was found to be around 17.7 % while the values obtained numerically were 16 %, 18 % and 20 % for $Co_2(OH)_3Cl$-H_2O nanofluid with spherical nanoparticles, mixed shapes and rhombus nanoplate, respectively. These results revealed that the increase in thermal conductivity of $Co_2(OH)_3Cl$-H_2O nanofluids at elevated temperatures could be more noticeable if surfactants were added to improve the nanoparticles' dispersion in the liquid and reduce clustering effects [99,100].

Conclusion

This study focuses on the preparation, characterisation, and utilisation of experimental and molecular dynamics (MD) simulation methods to examine the thermal conductivity of $Co_2(OH)_3Cl$-H_2O nanofluids under varying temperature, nanoparticle size, and shape conditions. Thermal conductivity analyses were conducted at a constant nanoparticle weight percentage of 0.03 wt % and within a temperature range spanning from 298 K to 318 K, with intervals of 5 K. The effect of changing propanol concentration on $Co_2(OH)_3Cl$ nanoparticles colour, size, shape and phase were reported. A mixture of $Co_{1.176}(OH)_2Cl_{0.348}(H_2O)_{0.456}$ and $Co_2(OH)_3Cl$ green hexagonal nanoplates were synthesised from 0 to 50 % propanol concentration. At 95 and 98 % propanol concentrations, pink $Co_2(OH)_3Cl$ nanospheres were formed while lavender β-phased $Co_2(OH)_3Cl$ nanospheres were produced at 70 and 100 %. In addition, at 100 % propanol, rhombus-shaped $Co_2(OH)_3Cl$ nanoplates were observed alongside the spherical nanoparticles. These findings confirm that increasing the propanol concentration reduces the size of $Co_2(OH)_3Cl$ nanoparticles and alters their shape. Interestingly, the thermal conductivity of nanofluids prepared with $Co_2(OH)_3Cl$ nanoparticles, with a diameter of 9.6 nm, showed a 17.7 % enhancement at a temperature of 318 K compared to pure water. To unravel the mechanisms behind the observed thermal conductivity

enhancement, computational calculations incorporating Equilibrium Molecular Dynamics (EMD) simulations along with the Green-Kubo (GK) method were employed to analyse $Co_2(OH)_3Cl$-H_2O nanofluids with extremely small particle sizes (< 10 nm) and different shapes (such as rhombus nanoplates and spherical shapes). The reported increase in thermal conductivity of 17.7 % was validated to be a result of the specific combination of nanoparticle shapes at extremely small particle sizes. The MD simulations confirmed the influence of particle shape on thermal conductivity as confirmed in a previous study which showed that the rods were better than the flowers. In our case, the rhombus nanoplates performed better than the spherical particles. The findings presented in this study confirmed that $Co_2(OH)_3Cl$ nanoparticles, produced via a low energy process (105.5 °C) can be used instead of Co_3O_4 nanoparticles in water as thermal fluids and performed similarly or better in comparison to past studies. Future studies will focus on conducting thermal conductivity measurements in the operating temperature range of medium solar thermal collectors. Measurements of thermophysical properties including density and specific heat capacity of nanofluids will be conducted. The effect of buoyancy forces on natural convection heat transfer in nanofluid flow within various cavity geometries, as well as the influence of activation energy at the solid–liquid interface, will be addressed in future research. Defects in nanoparticles and potential base liquids molecules adsorption on their surface were not considered in the model and will be integrated in DFT calculations in the future.

CRediT authorship contribution statement

P.T. Ntumba: Writing – original draft, Visualization, Methodology, Investigation, Data curation. **S. Khamlich:** Investigation, Methodology, Formal analysis, Resources, Software, Validation, Visualization, Writing – original draft. **B.T. Sone:** Validation, Writing – review & editing. **V. Fester:** Conceptualization, Project administration, Resources, Supervision, Validation, Writing – review & editing.

Declaration of competing interest

The authors declare that they have no known competing financial interests or personal relationships that could have appeared to influence the work reported in this paper.

Acknowledgements

The authors wish to acknowledge the technical support of the Flow Process & Rheology Centre (FPRC) and Cape Peninsula University of Technology, South Africa.

Data availability

Data supporting this study are openly available from figshare by accessing the link https://figshare.com/s/2b985aa8f085c864bbbb. Datafile is titled “Growth kinetics evaluation of hydrothermally synthesised $Co_2(OH)_3Cl$ nanoparticles for application in solar thermal heat transfer fluids” authored by Patricia Ntumba.

References

[1] S. Kakaç, Y. Yener, A. Pramuanjaroenkij, Convective Heat Transfer, 3rd ed., 2013.
[2] S.A. Kalogirou, Solar thermal collectors and applications, Prog. Energy Combust. Sci. 30 (3) (2004) 231–295.
[3] A. Shafieian, M. Khiadani, A. Nosrati, Strategies to improve the thermal performance of heat pipe solar collectors in solar systems: a review, Energy Convers. Manage 183 (2019) 307–331.
[4] N.I.S. Azha, H. Hussin, M.S. Nasif, T. Hussain, Thermal performance enhancement in flat plate solar collector solar water heater: a review, Processes 8 (7) (2020) 756.
[5] D. Del Col, A. Padovan, M. Bortolato, M. Dai Prè, E. Zambolin, Thermal performance of flat plate solar collectors with sheet-and-tube and roll-bond absorbers, Energy 58 (2013) 258–269.
[6] D. Missirlis, G. Martinopoulos, G. Tsilingiridis, K. Yakinthos, N. Kyriakis, Investigation of the heat transfer behaviour of a polymer solar collector for different manifold configurations, Renew. Energy 68 (2014) 715–723.
[7] S.U.S. Choi, J. Eastman, Enhancing thermal conductivity of fluids with nanoparticles. American Society of Mechanical Engineers, Fluids Engineering Division (Publication) FED, 1995, pp. 99–105.
[8] X.W. Lou, D. Deng, J.Y. Lee, J. Feng, Self-supported formation of needlelike Co_3O_4 nanotubes and their application as lithium-ion battery electrodes, Adv. Mater. 20 (2) (2008) 258–262.
[9] J. Park, X. Shen, G. Wang, Solvothermal synthesis and gas-sensing performance of Co_3O_4 hollow nanospheres, Sens. Actuators B: Chem. 136 (2) (2009) 494–498.
[10] Y. Chen, L. Hu, Novel Co_3O_4 porous polyhedrons derived from metal–organic framework toward high performance for electrochemical energy devices, J. Solid. State Chem. 239 (2016) 23–29.
[11] C. Lohaus, J. Morasch, J. Brötz, A. Klein, W. Jaegermann, Investigations on RF-magnetron sputtered Co_3O_4 thin films regarding the solar energy conversion properties, J. Phys. D. Appl. Phys. 49 (15) (2016) 155306.
[12] C. Ravi Dhas, R. Venkatesh, R. Sivakumar, A. Moses Ezhil Raj, C. Sanjeeviraja, Effect of solution molarity on optical dispersion energy parameters and electrochromic performance of Co_3O_4 films, Opt. Mater. 72 (2017) 717–729.
[13] M.Y. Nassar, I.S. Ahmed, Hydrothermal synthesis of cobalt carbonates using different counter ions: an efficient precursor to nano-sized cobalt oxide (Co_3O_4), Polyhedron. 30 (15) (2011) 2431–2437.
[14] W. Heuvel, B. Sone, V. Fester, Effect of cobalt complexes on cobalt oxide particles for the activation of peroxymonosulphate in textile wastewater treatment, Int. J. Environ. Sci. Technol. (2021) 1–16.
[15] H. Cui, M. Zayat, D. Levy, A chemical strategy to control the shape of oxide nanoparticles, J. Nanoparticle Res. 11 (6) (2009) 1331–1338.
[16] L. Yang, W. Guan, B. Bai, Q. Xu, Y. Xiang, Synthesis of yeast-assisted Co_3O_4 hollow microspheres—a novel biotemplating technique, J. Alloys. Compd. 504 (1) (2010) L10–L13.
[17] M. Mansournia, N. Rakhshan, Hydrothermal synthesis and tuning of size and morphology of α-$Co(OH)_2$ and α-$Co_2(OH)_3Cl$ nanostructures as precursors for nanosized Co_3O_4, Ceram. Int. 43 (9) (2017) 7282–7289.
[18] X. Meng, D. Deng, A new approach to facilely synthesize crystalline $Co_2(OH)_3Cl$ microstructures in an eggshell reactor system, CrystEngComm. 19 (21) (2017) 2953–2959.
[19] S. Ranganatha, S. Kumar, T.R. Penki, B. Kishore, N. Munichandraiah, $Co_2(OH)_3Cl$ xerogels with 3D interconnected mesoporous structures as a novel high-performance supercapacitor material, J. Solid. State Electrochem. 21 (1) (2017) 133–143.
[20] W. Feitknecht, G. Fischer, On the chemistry and morphology of basic salts of divalent metals III. About basic cobalt chlorides. (X. Communication on basic salts), Helv. Chim. Acta 18 (1) (1935) 555–569.
[21] W. Feitknecht, On the chemistry and morphology of the basic salts of divalent metals I. General considerations. (VIII. Communication on basic salts), Helv. Chim. Acta 18 (1) (1935) 28–40.
[22] P.M. de Wolff, The crystal structure of $Co_2(OH)_3Cl$, Acta Crystallogr. 6 (4) (1953) 359–360.
[23] H.R. Oswald, W. Feitknecht, About the hydroxide halides $me_2(OH)_3Cl$, -Br, -J of divalent metals (Me= Mg, Ni, Co, Cu, Fe, Mn), Helv. Chim. Acta 47 (1) (1964) 272–289.
[24] O. García-Martínez, P. Millán, R.M. Rojas, M.J. Torralvo, Cobalt basic salts as inorganic precursors of cobalt oxides and cobalt metal: thermal behaviour dependence on experimental conditions, J. Mater. Sci. 23 (4) (1988) 1334–1350.
[25] G. Wang, J. Liang, D. Li, M. Li, L. Li, Formation of hierarchical cobalt hydroxychloride nanostructures with enhanced performance for lithium-ion batteries, Cryst. Res. Technol. 57 (3) (2022) 2100133.
[26] J. Ma, T. Yuan, Y.S. He, J. Wang, W. Zhang, D. Yang, X.Z. Liao, Z.F. Ma, A novel graphene sheet-wrapped $Co2(OH)_3Cl$ composite as a long-life anode material for lithium ion batteries, J. Mater. Chem. A 2 (40) (2014) 16925–16930.
[27] X. Zhao, J. Li, J. Liu, L. Zhang, C. Yang, Graphene decorated by $Co_2(OH)_3Cl$: a promising lightweight wideband microwave absorber, J. Alloys. Compd. 811 (2019) 151905.
[28] Z. Wang, P. Hong, S. Peng, X. Zhang, T. Zou, Y. Yang, R. Zhao, Y. Wang, Hierarchitecture $Co_2(OH)_3Cl$@$FeCo_2O_4$ composite as a novel and high-performance electrode material applied in supercapacitor, Int. J. Energy Res. 44 (4) (2020) 3122–3133.
[29] H. Ma, Y. Zhang, L. Zhu, T. Majima, N. Wang, Efficient activation of peroxymonosulfate on cobalt hydroxychloride nanoplates through hydrogen bond for degradation of tetrabromobisphenol A, Chem. Eng. J. 413 (2021) 127480.
[30] A. Mariano, M.J. Pastoriza-Gallego, L. Lugo, L. Mussari, M.M. Piñeiro, Co_3O_4 ethylene glycol-based nanofluids: thermal conductivity, viscosity and high pressure density, Int. J. Heat. Mass Transf. 85 (2015) 54–60.
[31] V. Gupta, S. Sharma, U. Magotra, M. Sharma, Concentration and temperature dependent effects on acoustical parameters and thermal conductivity in cobalt oxide nanofluids, Prot. Met. Phys. Chem. Surf. 57 (6) (2021) 1198–1205.
[32] S. Rahman Salari, M. Khavarpour, M. Masoumi, S. Mosivand, Preparation of cobalt oxide and tin dioxide nanofluids and investigation of their thermophysical properties, Microfluid. Nanofluidics. 26 (10) (2022) 1–16.

[33] D.K. Devendiran, V.A. Amirtham, A review on preparation, characterization, properties and applications of nanofluids, Renew. Sustain. Energy Rev. 60 (2016) 21–40.

[34] R.M. Sarviya, V. Fuskele, Review on thermal conductivity of nanofluids, Mater. Today: Proc. 4 (2) (2017) 4022–4031.

[35] T. Sekhar, G. Nandan, R. Prakash, M. Muthuraman, Investigations on viscosity and thermal conductivity of cobalt oxide-water nano fluid, in: Materials Today: Proceedings, Elsevier Ltd, 2018, pp. 6176–6182.

[36] D. Mitra, K. Kumar Chattopadhyay, P. Chattopadhyay, Generation of stable thermal gradient by solar energy harvesting in porous cobalt oxide based nanofluid, Sustain. Energy Technol. Assess. 47 (2021) 101390.

[37] M. Alsboul, M.S.M. Ghazali, M.R. Gomaa, A. Albani, Experimental and theoretical investigation of the thermophysical properties of cobalt oxide (Co_3O_4) in distilled water (DW), ethylene glycol (EG), and DW-EG mixture nanofluids, Nanomaterials 12 (16) (2022) 2779.

[38] R.B. Manoram, R.S. Moorthy, Experimental investigation on energy and exergy analysis of solar water heating system using cobalt oxide based nanofluid, Heat. Mass Transf. 58 (1) (2022) 83–98.

[39] T.X. Phuoc, M. Massoudi, R.H. Chen, Viscosity and thermal conductivity of nanofluids containing multi-walled carbon nanotubes stabilized by chitosan, Int. J. Therm. Sci. 50 (1) (2011) 12–18.

[40] P. Garg, J.L. Alvarado, C. Marsh, T.A. Carlson, D.A. Kessler, K. Annamalai, An experimental study on the effect of ultrasonication on viscosity and heat transfer performance of multi-wall carbon nanotube-based aqueous nanofluids, Int. J. Heat. Mass Transf. 52 (21–22) (2009) 5090–5101.

[41] M. Xing, J. Yu, R. Wang, Thermo-physical properties of water-based single-walled carbon nanotube nanofluid as advanced coolant, Appl. Therm. Eng. 87 (2015) 344–351.

[42] M. Karami, M.A. Akhavan Bahabadi, S. Delfani, A. Ghozatloo, A new application of carbon nanotubes nanofluid as working fluid of low-temperature direct absorption solar collector, Sol. Energy Mater. Sol. Cells 121 (2014) 114–118.

[43] M.J. Assael, C.F. Chen, I. Metaxa, W.A. Wakeham, Thermal conductivity of suspensions of carbon nanotubes in water, Int. J. Thermophys. 25 (4) (2004) 971–985.

[44] B. Gu, B. Hou, Z. Lu, Z. Wang, S. Chen, Thermal conductivity of nanofluids containing high aspect ratio fillers, Int. J. Heat. Mass Transf. 64 (2013) 108–114.

[45] M.M. Ghosh, S. Ghosh, S.K. Pabi, Effects of particle shape and fluid temperature on heat-transfer characteristics of nanofluids, J. Mater. Eng. Perform. 22 (6) (2013) 1525–1529.

[46] T. He, D. Chen, X. Jiao, Controlled synthesis of Co_3O_4 nanoparticles through oriented aggregation, Chem. Mater. 16 (4) (2004) 737–743.

[47] A.A. Athawale, M. Majumdar, H. Singh, K. Navinkiran, Synthesis of cobalt oxide nanoparticles/fibres in alcoholic medium using γ-ray technique, Def. Sci. J. 60 (5) (2010) 507–513.

[48] M.R. Chowdhury, V. Fester, G. Kale, O. Cespedes, Hydrothermal precipitation of β-FeOOH nanostructure(s) in mixed solvent: study of their morphological and structural evolution, J. Nanoparticle Res. 16 (5) (2014) 1–11.

[49] S. Sarkar, R.P. Selvam, Molecular dynamics simulation of effective thermal conductivity and study of enhanced thermal transport mechanism in nanofluids, J. Appl. Phys. 102 (7) (2007).

[50] A. Loya, A. Najib, F. Aziz, A. Khan, G. Ren, K. Luo, Comparative molecular dynamics simulations of thermal conductivities of aqueous and hydrocarbon nanofluids, Beilstein. J. Nanotechnol. 13 (1) (2022) 620–628.

[51] T. Khamliche, S. Khamlich, M.K. Moodley, B.M. Mothudi, M. Henini, M. Maaza, Laser fabrication of Cu nanoparticles based nanofluid with enhanced thermal conductivity: experimental and molecular dynamics studies, J. Mol. Liq. 323 (2021) 114975.

[52] F. Jabbari, S. Saedodin, A. Rajabpour, Experimental investigation and molecular dynamics simulations of viscosity of CNT-water nanofluid at different temperatures and volume fractions of nanoparticles, J. Chem. Eng. Data 64 (1) (2019) 262–272.

[53] R. Zhang, S. Qing, X. Zhang, Z. Luo, Y. Liu, Investigation of different nanoparticles properties on the thermal conductivity and viscosity of nanofluids by molecular dynamics simulation, Nanotechnol. Rev. 12 (1) (2023).

[54] S.P. Shit, S. Pal, N.K. Ghosh, K. Sau, Enhanced thermophysical properties of water-based single and hybrid metallic nanofluids: insights from equilibrium molecular dynamics, Chem. Thermodyn. Therm. Anal. 8 (2022) 100096.

[55] H. Li, L. Wang, Y. He, Y. Hu, J. Zhu, B. Jiang, Experimental investigation of thermal conductivity and viscosity of ethylene glycol based ZnO nanofluids, Appl. Therm. Eng. 88 (2015) 363–368.

[56] H. Kurt, M. Kayfeci, Prediction of thermal conductivity of ethylene glycol–water solutions by using artificial neural networks, Appl. Energy 86 (10) (2009) 2244–2248.

[57] M.E. Tuckerman, Statistical Mechanics: Theory and Molecular Simulation (2nd Edition), Oxford University Press, 2023.

[58] M. Farzinpour, D. Toghraie, B. Mehmandoust, F. Aghadavoudi, A. Karimipour, Molecular dynamics study of barrier effects on Ferro- nanofluid flow in the presence of constant and time-dependent external magnetic fields, J. Mol. Liq. (2020) 308.

[59] T. Akiner, E. Kocer, J.K. Mason, H. Erturk, Green–Kubo assessments of thermal transport in nanocolloids based on interfacial effects, Mater. Today Commun. (2019) 20.

[60] D.A. McQuarrie, Statistical Mechanics, 12, University Science Books, Sausalito, Calif, 2000, p. 2004.

[61] W. Cui, Z. Shen, J. Yang, S. Wu, M. Bai, Influence of nanoparticle properties on the thermal conductivity of nanofluids by molecular dynamics simulation, RSC Adv. 4 (98) (2014) 55580–55589.

[62] H. Babaei, P. Keblinski, J.M. Khodadadi, Equilibrium molecular dynamics determination of thermal conductivity for multi-component systems, J. Appl. Phys. 112 (5) (2012).

[63] H. Matsubara, G. Kikugawa, M. Ishikiriyama, S. Yamashita, T. Ohara, Microscopic picture of heat conduction in liquid ethylene glycol by molecular dynamics simulation: difference from the monohydric case, Int. J. Heat. Mass Transf. 121 (2018) 1033–1038.

[64] R. Ma, Z. Liu, K. Takada, K. Fukuda, Y. Ebina, Y. Bando, T. Sasaki, Tetrahedral Co (II) coordination in α-type cobalt hydroxide: Rietveld refinement and X-ray absorption spectroscopy, Inorg. Chem. 45 (10) (2006) 3964–3969.

[65] Z. Zhao, F. Liang, P. Hu, L. Guo, Q. Zhong, L. He, C. Chen, Nanorods of ammine cobalt chloride $[Co(NH_3)_6Cl_3]$: synthesis, characterization, and magnetic properties, Phys. E: Low-Dimens. Syst. Nanostruct. 39 (1) (2007) 99–102.

[66] H. Zhang, Z. Yang, X. Zhang, N. Mao, Photocatalytic effects of wool fibers modified with solely TiO_2 nanoparticles and N-doped TiO_2 nanoparticles by using hydrothermal method, Chem. Eng. J. 254 (2014) 106–114.

[67] X.D. Liu, M. Hagihala, X.G. Zheng, W.J. Tao, D.D. Meng, S.L. Zhang, Q.X. Guo, Trimeric hydrogen bond in geometrically frustrated hydroxyl cobalt halogenides, Chin. Phys. Lett. 28 (1) (2011) 017803.

[68] K. Zenmyo, M. Tokita, Magnetic structure of geometrically frustrated compound $Co_2Cl(OH)_3$ determined by proton NMR, J. Magn. Magn. Mater. 321 (14) (2009) 2192–2196.

[69] X.D. Liu, D.D. Meng, M. Hagihala, X.G. Zheng, Q.X. Guo, Raman and mid-infrared spectroscopic study of geometrically frustrated hydroxyl cobalt halides at room temperature, Chin. Phys. B 20 (7) (2011) 077801.

[70] Z. Zhao, F. Geng, J. Bai, H.M. Cheng, Facile and controlled synthesis of 3D nanorods-based urchinlike and nanosheets-based flowerlike cobalt basic salt nanostructures, J. Phys. Chem. C 111 (10) (2007) 3848–3852.

[71] M. Aghazadeh, S. Dalvand, M. Hosseinifard, Facile electrochemical synthesis of uniform β-$Co(OH)_2$ nanoplates for high performance supercapacitors, Ceram. Int. 40 (2) (2014) 3485–3493.

[72] M. Chowdhury, V. Fester, G. Kale, Growth kinetics evaluation of hydrothermally synthesized β-FeOOH nanorods, J. Cryst. Growth 387 (2014) 57–65.

[73] H. Xie, J. Wang, T. Xi, Y. Liu, Thermal conductivity of suspensions containing nanosized SiC particles, Int. J. Thermophys. 23 (2) (2002) 571–580.

[74] S.M.S. Murshed, K.C. Leong, C. Yang, A combined model for the effective thermal conductivity of nanofluids, Appl. Therm. Eng. 29 (11–12) (2009) 2477–2483.

[75] J. Jeong, C. Li, Y. Kwon, J. Lee, S.H. Kim, R. Yun, Particle shape effect on the viscosity and thermal conductivity of ZnO nanofluids, Int. J. Refrig. 36 (8) (2013) 2233–2241.

[76] P.B. Maheshwary, C.C. Handa, K.R. Nemade, A comprehensive study of effect of concentration, particle size and particle shape on thermal conductivity of titania/water based nanofluid, Appl. Therm. Eng. 119 (2017) 79–88.

[77] V. Ganesan, C. Louis, S.P. Damodaran, Novel nanofluids based on magnetite nanoclusters and investigation on their cluster size-dependent thermal conductivity, J. Phys. Chem. C 122 (12) (2018) 6918–6929.

[78] S. Khamlich, J. Jakobi, T. Khamliche, F. Ismail, O. Nemraoui, C. Rehbock, V. Fester, S. Barcikowski, Enhanced heat transfer of laser-fabricated copper nanofluid at ultra-low concentration driven by the nanoparticle surface area, J. Mol. Liq. 383 (2023) 122104.

[79] N. Ali, J.A. Teixeira, A. Addali, A review on nanofluids: fabrication, stability, and thermophysical properties, J. Nanomater. (2018). , 2018.

[80] X. Wang, X. Xu, S.U.S. Choi, Thermal conductivity of nanoparticle-fluid mixture, J. Thermophys. Heat Transf. 13 (4) (1999) 474–480.

[81] S.M.S. Murshed, K.C. Leong, C. Yang, Investigations of thermal conductivity and viscosity of nanofluids, Int. J. Therm. Sci. 47 (5) (2008) 560–568.

[82] A.R. Moghadassi, S.M. Hosseini, D.E. Henneke, Effect of CuO nanoparticles in enhancing the thermal conductivities of monoethylene glycol and paraffin fluids, Ind. Eng. Chem. Res. 49 (4) (2010) 1900–1904.

[83] A. Riahi, S. Khamlich, M. Balghouthi, T. Khamliche, T.B. Doyle, W. Dimassi, A. Guizani, M. Maaza, Study of thermal conductivity of synthesized Al_2O_3-water nanofluid by pulsed laser ablation in liquid, J. Mol. Liq. 304 (2020) 112694.

[84] Y. Xuan, Q. Li, W. Hu, Aggregation structure and thermal conductivity of nanofluids, AIChE J. 49 (4) (2003) 1038–1043.

[85] T.P. Teng, Y.H. Hung, T.C. Teng, H.E. Mo, H.G. Hsu, The effect of alumina/water nanofluid particle size on thermal conductivity, Appl. Therm. Eng. 30 (14–15) (2010) 2213–2218.

[86] J.H. Lee, S.H. Lee, S. Pil Jang, Do temperature and nanoparticle size affect the thermal conductivity of alumina nanofluids? Appl. Phys. Lett. 104 (16) (2014).

[87] L. Zheng, M. Chen, Z. Sun, H.Y. Ko, B. Santra, P. Dhuvad, X. Wu, Structural, electronic, and dynamical properties of liquid water by ab initio molecular dynamics based on SCAN functional within the canonical ensemble, J. Chem. Phys. 148 (16) (2018).

[88] Y.S. Lin, P.Y. Hsiao, C.C. Chieng, Constructing a force interaction model for thermal conductivity computation using molecular dynamics simulation: ethylene glycol as an example, J. Chem. Phys. 134 (15) (2011).

[89] T. Mohorič, U. Bren, V. Vlachy, Effects of translational and rotational degrees of freedom on the hydration of ionic solutes as seen by the popular water models, Acta Chim. Slov. 62 (3) (2015) 489–497.

[90] A. Alkhwaji, S. Elbahloul, M.Z. Abdullah, K.F.B.A. Bakar, Selected water thermal properties from molecular dynamics for engineering purposes, J. Mol. Liq. 324 (2021) 114703.

[91] D. Bertolini, A. Tani, Thermal conductivity of water: molecular dynamics and generalized hydrodynamics results, Phys. Rev. E 56 (4) (1997) 4135.
[92] X. Guo, X. Chen, J. Zhao, W. Zhou, J. Wei, Effect of the addition of graphene nanoplatelets on the thermal conductivity of rocket kerosene: a molecular dynamics study, Materials 15 (16) (2022) 5511.
[93] S. Mukherjee, P.C. Mishra, P. Chaudhuri, S. Chakraborty, Contributory effect of diffusive heat conduction and Brownian motion on thermal conductivity enhancement of nanofluids, Pramana - J. Phys. 94 (1) (2020).
[94] S.M. Nyamgoudar, V.P. Silaparasetti, M.P. Shilpa, K.S. Pavithra, S. Mundinamani, K.M. Eshwarappa, S. Surabhi, K. Ramam, A. Ravikirana, Ganesha, S. C Gurumurthy, Analysis of shape dependency of thermal conductivity of silver-based nanofluids, J. Therm. Anal. Calorim. 147 (24) (2022) 14031–14038.
[95] H. Aybar, M. Sharifpur, M.R. Azizian, M. Mehrabi, J.P. Meyer, A review of thermal conductivity models for nanofluids, Heat Transf. Eng. 36 (13) (2015) 1085–1110.
[96] Z. Liu, Y. Zhu, R.R. Rao, J.R. Clausen, C.K. Aidun, Nanoparticle transport in cellular blood flow, Comput. Fluids 172 (2018) 609–620.
[97] A. Hashim, Hamid, M. Khan, Heat and mass transport phenomena of nanoparticles on time-dependent flow of Williamson fluid towards heated surface, Neural Comput. Appl. 32 (8) (2020) 3253–3263.
[98] F. Jabbari, A. Rajabpour, S. Saedodin, Thermal conductivity and viscosity of nanofluids: a review of recent molecular dynamics studies, Chem. Eng. Sci. 174 (2017) 67–81.
[99] M.C. Mbambo, S. Khamlich, T. Khamliche, M.K. Moodley, K. Kaviyarasu, I. G. Madiba, M.J. Madito, M. Khenfouch, J. Kennedy, M. Henini, E. Manikandan, M. Maaza, Remarkable thermal conductivity enhancement in Ag—decorated graphene nanocomposites based nanofluid by laser liquid solid interaction in ethylene glycol, Sci. Rep. 10 (1) (2020) 1–14. *2020 10:1*.
[100] G. Xia, H. Jiang, R. Liu, Y. Zhai, Effects of surfactant on the stability and thermal conductivity of Al_2O_3/de-ionized water nanofluids, Int. J. Therm. Sci. 84 (2014) 118–124.